

KfK 3094
Dezember 1980

^{176}Lu : Cosmic Clock or Stellar Thermometer?

H. Beer, F. Käppeler, K. Wisshak, R. A. Ward
Institut für Angewandte Kernphysik

Kernforschungszentrum Karlsruhe

KERNFORSCHUNGSZENTRUM KARLSRUHE
Institut für Angewandte Kernphysik

KfK 3094

^{176}Lu : Cosmic Clock or Stellar Thermometer ?

H. Beer, F. Käppeler, K. Wisshak, and R.A. Ward*

Kernforschungszentrum Karlsruhe GmbH, Karlsruhe

*Max-Planck-Institut für Physik und Astrophysik,
Institut für Astrophysik

Als Manuskript vervielfältigt
Für diesen Bericht behalten wir uns alle Rechte vor

Kernforschungszentrum Karlsruhe GmbH
ISSN 0303-4003

Abstract

We quantitatively examine the various experimental and theoretical aspects of the stellar synthesis of the long-lived ground state of ^{176}Lu (3.6×10^{10} y). We discuss the various regimes of stellar temperature and free-neutron density in which either: (i) the internal electromagnetic couplings between $^{176}\text{Lu}^o$ and $^{176}\text{Lu}^m$ (3.68 hours) are sufficiently slow that they may be treated as separate nuclei, or (ii) the internal couplings are rapidly able to establish thermal equilibrium between $^{176}\text{Lu}^o$ and $^{176}\text{Lu}^m$. Case (i) above allows $^{176}\text{Lu}^o$ to be used as a cosmic clock of galactic s-process nucleosynthesis. As experimental input to the cosmic clock, we have measured the 30-keV neutron capture cross sections: $\sigma(^{170}\text{Yb}) = 766 \pm 30$ mb and $\sigma(^{175}\text{Lu}) = 1266 \pm 43$ mb. This latter value also yields the branching ratio, B, to $^{176}\text{Lu}^o$ from neutron capture on ^{175}Lu as: $B(24 \text{ keV}) = 0.362 \pm 0.038$. Using abundance and cross-section systematics, we derive an upper limit on the mean s-process age of solar material of 11×10^9 y before the solidification of the meteorites. By requiring the solar abundance of ^{170}Yb to be consistent with these same σN systematics, we can also bracket the allowable range for the averages s-process neutron density as: $10^7 \text{ cm}^{-3} \lesssim \langle n \rangle \lesssim 4 \times 10^7 \text{ cm}^{-3}$. However, for sufficiently high stellar temperatures, case (ii) above implies that the total effective half-life of ^{176}Lu against beta decay becomes a very strong function of the stellar temperature: $t_{1/2}(^{176}\text{Lu}) = 18.5 \exp(14.7/T_8)$ hours for $T_8 > 1$, and thus the $^{176}\text{Lu} \rightarrow ^{176}\text{Hf}$ decay would constitute a sensitive stellar s-process thermometer. We show that the fact that ^{176}Lu does exist in the solar system can place firm constraints on the temperature and neutron density of current models for the site of the s-process. Our preliminary studies indicate that the decay of $^{176}\text{Lu}^o$ can be unambiguously used as a cosmic clock of nucleosynthesis only if the s-process occurs in nature at temperatures $T_8 < 1.9$.

ZUSAMMENFASSUNG

Die verschiedenen experimentellen und theoretischen Seiten der stellaren Synthese des langlebigen Grundzustands von ^{176}Lu (3.6×10^{10} a) werden untersucht. Wir diskutieren verschiedene Systeme stellarer Temperatur und freier Neutronendichte, in denen entweder (i) die internen elektromagnetischen Kopplungen zwischen $^{176}\text{Lu}^0$ und $^{176}\text{Lu}^m$ (3.68 h) ausreichend langsam sind, so daß sie als getrennte Kerne behandelt werden dürfen oder (ii) in denen die internen Kopplungen schnell ein thermisches Gleichgewicht zwischen $^{176}\text{Lu}^0$ und $^{176}\text{Lu}^m$ herstellen können. Die erste Annahme erlaubt es, den Zerfall von $^{176}\text{Lu}^0$ als kosmische Uhr der galaktischen s-Prozeßsynthese zu benutzen. Als experimentelle Bestimmungsgröße für die kosmische Uhr haben wir die 30 keV Einfangquerschnitte $\sigma(^{170}\text{Yb}) = 766 \pm 30$ mb und $\sigma(^{175}\text{Lu}) = 1266 \pm 43$ mb gemessen. Dieser letztere Wert ergibt auch das Verzweungsverhältnis, mit dem $^{176}\text{Lu}^0$ beim Neutroneneinfang in ^{175}Lu gebildet wird: $B = (24 \text{ keV}) = 0.362 \pm 0.038$. Mit Hilfe der Häufigkeits- und Querschnittssystematik leiten wir eine obere Grenze für das mittlere s-Prozeßalter der solaren Materie von 12×10^9 a vor der Verfestigung der Meteorite ab. Mit der Forderung, daß die solare Häufigkeit von ^{170}Yb konsistent mit dieser gleichen σN Systematik sein soll, können wir den erlaubten Bereich für die mittlere s-Prozeß Neutronendichte auf $10^7 \text{ cm}^{-3} \lesssim \langle n \rangle \lesssim 4 \times 10^7 \text{ cm}^{-3}$ eingrenzen. Für genügend hohe stellare Temperaturen hat Fall (ii) zur Folge, daß die totale effektive Halbwertszeit von ^{176}Lu gegen Betazerfall eine sehr starke Funktion der stellaren Temperatur wird: $t_{1/2}(^{176}\text{Lu}) = 18.5 \exp(14.7/T_8)$ Stunden für $T_8 > 1$. Somit würde der $^{176}\text{Lu} \rightarrow ^{176}\text{Hf}$ Zerfall ein empfindliches stellares Thermometer für den s-Prozeß bilden. Die Tatsache, daß ^{176}Lu im solaren System existiert, hat starke Einschränkungen für die Temperatur und Neutronendichte der geläufigen Modelle über die Lage des s-Prozesses zur Folge. Unsere vorläufigen Untersuchungen zeigen, daß der Zerfall von $^{176}\text{Lu}^0$ nur dann eindeutig als kosmische Uhr der Nukleosynthese benutzt werden kann, wenn der s-Prozeß in der Natur bei Temperaturen $T_8 < 1.9$ abläuft.

I. INTRODUCTION

The advantage of long-lived galactic clocks is that their very weak radioactivities are capable effectively of integrating over any short-term irregularities in galactic nucleosynthesis and thereby can provide an average age for a particular type of stellar nucleosynthesis (Clayton 1964; Schramm and Wasserburg 1970). To this end, the 36 billion year half-life of the ground state of ^{176}Lu makes it unique in its potential for giving an independent clock for s-process nucleosynthesis that is not clouded by any contributions from r-process beta decays. The situation for ^{176}Lu was first discussed in detail by Audouze, Fowler, and Schramm (1972) and independently by Arnould (1973) with regards to its use as a galactic cosmochronometer. Later discussions were also given by Ward, Newman, and Clayton (1976), McCulloch, De Laeter, and Rosman (1976), Ward (1977), Ward and Newman (1978), and most recently by Beer and Käppeler (1980).

However, unlike the situation with the other long-lived chronometers for r-process nucleosynthesis, the decay of ^{176}Lu is complicated by the fact that its isomeric state at 127 keV beta decays to stable ^{176}Hf with a half-life of only 3.68 hours. Therefore, if this short-lived isomer and the ground state can be rapidly linked internally via collisions with surrounding hot photons and/or charged particles in the synthesizing stellar plasma, then the resulting thermal distribution of level populations yields a dramatically lower overall half-life against beta decay (Ward, Newman, and Clayton 1976; Ward 1977; Ward and Newman 1978). Under these conditions, the abundances of s-only ^{176}Lu and s-only ^{176}Hf are very sensitive functions of the stellar temperature and free-neutron density. Therefore, depending on the details of internal electromagnetic transitions among the excited states of ^{176}Lu , the decay $^{176}\text{Lu} \rightarrow ^{176}\text{Hf}$ would constitute a stellar thermometer for the s-process.

On the other hand, if the (direct or indirect) transition rates between $^{176}\text{Lu}^o$ and $^{176}\text{Lu}^m$ are sufficiently slow, then one needs only the fraction of 30-keV neutron captures on ^{175}Lu that directly yield ^{176}Lu ; and the resulting separate identities of $^{176}\text{Lu}^o$ and $^{176}\text{Lu}^m$ allow the formalism of Audouze, Fowler, and Schramm (1972), Arnould (1973), and

Beer and Käppeler (1980) to be used in obtaining a cosmic clock from the slow decay of $^{176}\text{Lu}^o$.

In Figure 1 we have schematically shown the various s-, p-, and r-process contributions to the nuclei from $A = 166$ to $A = 180$, including the possible branchings (Ward, Newman, and Clayton 1976; Ward and Newman 1978) encountered in the s-process path at ^{170}Tm , ^{171}Tm , as well as ^{176}Lu . The s-process path is indicated by the solid line in the valley of beta stability, and the final beta decays of the much more neutron-rich r-process species are indicated by the diagonal dashed lines. In the work that follows, we will focus our attention on the nuclear systematics of stellar nucleosynthesis for the s-only isotopes: ^{170}Yb , ^{176}Lu , and ^{176}Hf . In particular, we will try to clarify the situation concerning the s-process synthesis of these nuclei and their relation to the development of a cosmochronometer based on ^{176}Lu .

In §II we will describe our experimental contributions to the input nuclear physics of the problem by measuring the neutron capture cross sections: $^{170}\text{Yb}(n,\gamma)^{171}\text{Yb}$ and $^{175}\text{Lu}(n,\gamma)^{176}\text{Lu}^{o+m}$. These detailed laboratory measurements will then enable us to examine the systematics of the solar system σN curve beyond the shell closing at 82 neutrons in the $140 < A < 190$ mass region, where the cross-section-times-abundance of s-only isotopes is expected (in the absence of branching) to be a slowly decreasing function of the atomic weight. Also, our result for $^{175}\text{Lu}(n,\gamma)^{176}\text{Lu}^{o+m}$ can be combined with the earlier measurement of Beer and Käppeler (1980) of the $^{175}\text{Lu}(n,\gamma)^{176}\text{Lu}^m$ cross section to obtain accurately the fraction of 30-keV s-process neutron captures by ^{175}Lu that leave ^{176}Lu in its long-lived (chronologically interesting!) ground state.

In §III we will discuss the various stellar regimes in which the $^{176}\text{Lu} \rightarrow ^{176}\text{Hf}$ decay constitutes either a cosmic clock for galactic s-process nucleosynthesis or a stellar thermometer of s-processing stellar models. A discussion will also be given of the uncertainties and needed improvements in input nuclear physics and abundance measurements that form the basis of the s-process systematics for the $140 < A < 190$ mass range of solar system elements.

Finally, in §IV we will apply our general techniques for examining the stellar synthesis of the nuclei ^{170}Yb , ^{176}Lu , and ^{176}Hf to a detailed stellar model for the thermodynamic environment of the s-process. For this model, we have used the published (Iben 1977; Cosner, Iben, and Truran 1980) characteristics of a $7-M_{\odot}$ red giant star with a $1.16-M_{\odot}$ carbon-oxygen core, that is undergoing the helium shell-flashing stage of stellar evolution. We critically discuss the resulting "freeze-out" characteristics of such a model for producing the solar system's abundances of ^{170}Yb , ^{176}Lu , and ^{176}Hf .

II. EXPERIMENT

a) Measurement

The neutron source and the experimental set up were almost the same as reported elsewhere (Wisshak and Käppeler 1978 and 1979; Beer, Käppeler, and Wisshak 1979). Therefore, only a brief description of the experiment is given here. The measurements were carried out at the Karlsruhe pulsed 3 MV Van de Graaff accelerator. Neutrons were generated via the ${}^7\text{Li}(p,n)$ and ${}^3\text{H}(p,n)$ reactions with proton energies at 20 keV and 100 keV above the reaction threshold, respectively, to obtain a kinematically collimated neutron beam in the entire energy range from 5 to 200 keV. The scheme of the experimental set up is displayed in Figure 2. The proton beam impinges on a water cooled Li or ${}^3\text{H}$ target with a diameter of 6 mm. The samples are located at flight paths of 68 mm, and the neutron energy is measured by the time-of-flight technique. The time resolution of 1.2 to 1.3 ns allowed for a reasonable energy resolution. The geometry of the arrangement and the kinematics of the ${}^7\text{Li}$ and ${}^3\text{H}$ reactions were optimized to keep all massive parts of the experiment outside the cone of the primary neutron flux.

A set of six samples was mounted with thin wires on the light-weight aluminum frame of a sample changer and moved into the neutron beam in a direction perpendicular to the plane of Figure 2. The cycle time was chosen short enough (~ 1 h) that long term variations of the neutron yield were averaged out completely. The yield was determined by a beam current integrator and controlled by a ${}^6\text{Li}$ -glass flux monitor at 20 deg with respect to the beam axis. A ${}^6\text{Li}$ -glass transmission detector at a flight path of 93.5 cm served to adjust and control the maximum neutron energy. The prompt capture gamma rays were recorded with a Moxon-Rae detector at a 120 deg backward angle, completely outside the neutron cone. Lead shielding is used between the Moxon-Rae detector and the target to reduce the prompt gamma flash. The Moxon-Rae detector consists of a 2.5 cm thick graphite converter and a NE111 plastic scintillator (0.5 mm thick, 90 mm diameter) with a Valvo XP2041 photomultiplier tube. The essential characteristic of the Moxon-Rae detector is that its efficiency increases linearly with gamma-ray energy. Therefore, the efficiency of a capture event is proportional to the neutron separation energy of the investigated compound nucleus and is thereby independent of the details

of each capture gamma-ray cascade (Moxon and Rae 1963). In Table 1 some important parameters of the experiment are summarized.

The six samples that were used each had a diameter of 30 mm and were contained in 0.1 mm thick Al-cannings. They consisted in particular of:

1. natural Lu,
2. natural Yb,
3. Yb enriched in ^{170}Yb to 78.78%,
4. ^{197}Au (The gold capture cross section was used as a standard),
5. graphite (This sample served as a pure scatterer. The thickness was adjusted to the Au scattering cross section.),
6. an empty sample container to correct for background events.

In Table 2 a compilation of the sample data is given.

For each sample position, a time-of-flight (TOF) spectrum of 1024 channels was recorded for both the Moxon-Rae and the 0 deg transmission detector, whereas a 1024 channel pulse height spectrum was taken for the 20 deg flux monitor. All of these spectra were written sequentially on magnetic tape. The Moxon-Rae TOF spectra for lutetium and the corresponding background as shown in Figure 2 represent the sum over all experimental cycles. One finds that a sufficient signal-to-background ratio was achieved at the relevant neutron energies.

b) Data analysis

To remove long-term drifts in the electronics (indicated by slight alterations of the prompt gamma-ray peak), the individual spectra of each sample were linearly shifted to one common gamma-ray peak position prior to the formation of the summed spectra. In addition, a transformation to a common flight path had to be carried out to take care of flight path differences, ΔL , which are present among the individual samples ($\Delta L \leq 1.4$ mm) and are also introduced via the replacement of the exhausted neutron targets ($\Delta L \leq 0.5$ mm). These flight path differences do not correspond to the flight path uncertainties which are only ± 0.2 mm. In calculating the neutron energy by means of the TOF technique, the dimensions of the samples are large enough to yield different flight paths for the center and the peripheral parts. An effective flight path, L_{eff} , was determined

according to the relation $L_{\text{eff}} = \frac{2}{3R^2} \left[\sqrt{(R^2 + L^2)^3} - L^3 \right]$ where R is the sample radius and L the distance between neutron target and sample center. The effective flight path is about 1.3% larger than the distance L.

As the measuring time for each sample was defined by integration of the proton beam current falling on the neutron target, a normalization to the observed neutron flux was carried out. These corrections are in general much smaller than the extreme values of 1.3% and 0.4% for runs with the ${}^7\text{Li}(p,n)$ and the ${}^3\text{H}(p,n)$ reaction, respectively. The background spectrum measured with the empty sample canning was subtracted from the mean spectra. No background correction for neutrons scattered in the sample was required because no difference could be detected between the spectrum of the empty sample canning and the spectrum with the carbon scatterer.

The capture cross section was then determined from the TOF spectra by

$$\frac{C_x}{C_{\text{Au}}} = \frac{N_x}{N_{\text{Au}}} \cdot \frac{(\text{MS} \cdot \text{SS})_x}{(\text{MS} \cdot \text{SS})_{\text{Au}}} \cdot \frac{K_x}{K_{\text{Au}}} \cdot \frac{\sum_i \sigma_i H_i (E_{\text{Bi}} + E_n)}{\sigma_{\text{Au}} (E_{\text{BAu}} + E_n)}, \quad (1)$$

where C_i denotes the background subtracted count rates, (MS·SS) the corrections for neutron multiple scattering and self-shielding, N the sample thickness in atoms per barn, and K the correction for gamma-ray absorption in the sample. The subscripts x and Au refer to the sample under investigation and the gold reference sample. The index i stands for the various isotopes of the sample. H designates the isotopic abundance, E_B is the neutron binding and E_n the neutron kinetic energy. The correction factors (MS·SS) were determined by the Monte Carlo code SESH (Fröhner 1968) which operates with level statistics adequate for the present nuclei with high level densities. The gamma-ray absorption correction K was estimated using the total energy absorption cross section tabulated in Storm and Israel (1970). Above 1 MeV the correction was found to be nearly energy-independent. The numerical values for (MS·SS) and for K are included in Table 2.

c) Results

The cross sections were calculated in energy increments corresponding to the time resolution of the Moxon-Rae detector. However, in the energy

region below 10 keV, larger energy intervals were chosen to improve statistics. The isotopic impurities in the ^{170}Yb and the ^{175}Lu samples were taken into account using the data of Shorin, Kononov, and Poletaev (1974), Beer and Käppeler (1980), and Macklin and Gibbons (1967), respectively. For the calculation of the capture cross section of natural Yb and Lu: $\sigma = \sum_i \sigma_i H_i$, an effective neutron binding energy $E_f = \sum_i \sigma_i H_i (E_{Bi} + E_n) / \sum_i \sigma_i H_i$ was defined. The results of the measurements are tabulated in the Appendix. The various contributions to the total systematic uncertainty were evaluated carefully (see for example Wiss-hak and Käppeler 1978 and 1979) and are listed in Table 3. It should be noted that the overall systematic uncertainty obtained with this method does not exceed 4%.

The cross sections are plotted in Figure 3 together with data from previous work. The present results are indicated as full black circles for RUNI with $^7\text{Li}(p,n)$ and as squares for RUNII with $^3\text{H}(p,n)$. The solid lines represent least squares fits of the present data using the statistical model code FITACS (Fröhner 1980). The parametrization of the cross section in terms of s-, p- and d-wave neutron strength functions and of average level density and radiation width delivered by the code are given in Table 4. This parametrization represents a reasonable means of extrapolating the cross section to neutron energies below 5 keV and above 200 keV.

For ^{175}Lu and ^{170}Yb , the measurements of Macklin and Gibbons (1967) and Allen and Cohen (1979) are in fair agreement with the present data. Unfortunately, the 30 keV cross section for ^{175}Lu reported by Macklin and Gibbons (1967) which was used in the literature for the Maxwellian average cross section, shows the largest discrepancy (20%) compared to our results and this has a strong influence on the ^{176}Lu cosmic clock (Beer and Käppeler 1980). The measurements of Block et al. (1961), Konks, Popov, and Fenin (1968), and Lépine, Douglas, and Maia (1972) for natural Lu are in reasonable agreement with the natural Lu cross section; however, the data of Gibbons and Macklin (1961) systematically deviate by a large factor. The Yb measurements of Block et al. (1961) and Lépine, Douglas, and Maia (1972) show deviations only at certain energies compared to our measurement. The isotopic cross sections $^{171}, ^{172}, ^{173}, ^{174}, ^{176}\text{Yb}$

of Shorin, Kononov, and Poletaev (1974) can be combined to obtain an average natural cross section (including a correction for ^{170}Yb with our result), and the resulting cross section is in excellent agreement with our measured natural Yb cross section. As ^{171}Yb is responsible for 40% of the natural Yb cross section and is also the major impurity in our ^{170}Yb sample (10.54%), this agreement between Shorin, Kononov, and Poletaev (1974) and our result gives us confidence in the reliability of our corrections for isotopic impurities.

Our microscopic cross sections given in the Appendix were used to calculate Maxwellian averaged cross sections $\langle\sigma\rangle$ at various thermal temperatures kT according to:

$$\langle\sigma\rangle = \frac{2}{\sqrt{\pi}} \frac{\int_{E_1}^{E_2} \sigma E \exp(-E/kT) dE}{\int_{E_1}^{E_2} E \exp(-E/kT) dE} \quad (2)$$

In principle, the limits of integration E_1 , E_2 reach from 0 to ∞ . However, for thermal energies of $kT \sim 30$ keV the effective range of the neutron energy lies between 1 keV and 300 keV. The main contributions arise from the measured range 5 to 200 keV so that the rest can be covered with sufficient accuracy by the statistical model extrapolation. The results from $kT = 10$ to 100 keV for ^{170}Yb and ^{175}Lu are summarized in Table 5.

III. DISCUSSION

a) ^{176}Lu , a cosmic clock

^{176}Lu with a half-life of $(3.6 \pm 0.16) \times 10^{10}$ yr represents one of the relics of radioactive material which has survived since the formation of the heavy elements. ^{176}Lu is shielded against r-process contributions by the stable isobar ^{176}Yb (Figure 1) and hence it was formed only by the s-process. Therefore, it is possible from s-process systematics to calculate how many ^{176}Lu nuclei were originally created in stars. The comparison of that original abundance, $N^*(^{176}\text{Lu})$, with the abundance $N^\circ(^{176}\text{Lu})$ observed in the solar system offers then the possibility of evaluating the age of ^{176}Lu - and herewith the age of the s-process - from the ^{176}Lu half-life. Although the production rate of s-process matter cannot be expected to be uniform in time, Schramm and Wasserburg (1970) have shown that such fluctuations can be neglected if a long-lived isotope like ^{176}Lu is used as a clock. Therefore, in this case the mean s-process age $\langle T \rangle$ is given simply by:

$$\langle T \rangle = \frac{1}{\lambda} \ln \left[\frac{N^*(^{176}\text{Lu})}{N^\circ(^{176}\text{Lu})} \right] \quad (3)$$

$$\text{with } N^*(^{176}\text{Lu}) = B \cdot N(^{176}\text{Lu}), \quad (4)$$

where λ denotes the decay rate of ^{176}Lu , and the factor B takes into account that only a fraction of the total amount of synthesized nuclei with mass number 176 is formed in the ground state of ^{176}Lu . The residual part populates the 3.68 h isomeric state in ^{176}Lu which in the s-process time scale decays completely to ^{176}Hf (Figure 4). From equation (3), the mean s-process age $\langle T \rangle$ can be evaluated if the ratio $N^*(^{176}\text{Lu}) / N^\circ(^{176}\text{Lu})$ is known. The branching ratio B is determined by the probability for populating the ground state via neutron capture on ^{175}Lu :

$$B = \frac{\sigma^o(^{175}\text{Lu})}{\sigma(^{175}\text{Lu})} = 1 - \frac{\sigma^m(^{175}\text{Lu})}{\sigma(^{175}\text{Lu})}, \quad (5)$$

where $\sigma(^{175}\text{Lu})$ represents the Maxwellian averaged capture cross section of ^{175}Lu and $\sigma^o(^{175}\text{Lu})$, $\sigma^m(^{175}\text{Lu})$ are its two components leading to the ground and isomeric state in ^{176}Lu . With our result for $\sigma(^{175}\text{Lu})$ and the measure-

ment of $\sigma^m(^{175}\text{Lu})$ by Beer and Käppeler (1980), the important quantity B was found to be $B = 0.362 \pm 0.038$ at 24 keV.

In principle, the original abundance $N^*(^{176}\text{Lu})$ can be derived via the dependence of σN on atomic weight from ^{170}Yb , a nearby stable s-only nucleus for which we have also determined the neutron capture cross section. However, in comparing the observed σN value of ^{170}Yb with the rest of the solar system σN curve one must be careful to allow for the fact that in various s-process environments there may be significant competition between neutron capture and beta-decay at radioactive ^{170}Tm ($t_{1/2} = 0.35$ years). Thus, in some s-process regimes, ^{170}Yb may be formed in part as its progenitor ^{170}Tm , and we must include the subsequent decay of ^{170}Tm in the observed abundance today of ^{170}Yb . This effect is important because of the fact that the capture cross section of ^{170}Tm (being an odd-odd nucleus) will be much larger than that of its daughter ^{170}Yb (see Table 6). In the extreme case that the s-process neutron flux is so strong that ^{170}Tm can always capture a neutron before beta-decaying, we see that using only the cross section of ^{170}Yb in forming the σN value at $A = 170$ would result in a yield smaller than the actual case by the ratio $\sigma(^{170}\text{Yb})/\sigma(^{170}\text{Tm})$. Therefore, one must be careful in extrapolating the observed yield at s-only ^{170}Yb out to ^{176}Lu .

To assess quantitatively this effect we can use the formalism developed by Ward, Newman, and Clayton (1976) for an exponential distribution of s-process neutron fluences to obtain correctly this extrapolation when we also allow for the possibility of s-process branching at ^{170}Tm and at ^{171}Tm ($t_{1/2} = 1.92$ years) as shown in Figure 1. We include this latter possibility for completeness although its effect will not be so pronounced because ^{171}Tm does not decay to a shielded s-only isobar. All of the other beta-decay times encountered along the chain between $A = 170$ and $A = 176$ appear to be too short to cause any further significant branching for reasonable s-process neutron fluxes. Therefore, under the assumption of a steady s-process neutron irradiation, we obtain the following result for the theoretical s-process yield at ^{176}Lu in terms of the observed σN values of ^{170}Yb and ^{176}Lu :

$$\frac{N^*(^{176}\text{Lu})}{N^\circ(^{176}\text{Lu})} = \left[\frac{1}{f_n} + \frac{1}{\tau_o \sigma(^{176}\text{Lu})} \right]^{-1} \prod_{i=^{172}\text{Yb}}^{^{175}\text{Lu}} \zeta(i)$$

$$\times \left[\left[1 + \frac{1-f_{171}}{\tau_o \sigma(^{171}\text{Tm})} \right]^{-1} \{ 1+f_{171} [\zeta(^{171}\text{Yb})-1] \} \right. \\ \left. + \zeta(^{170}\text{Yb}) \zeta(^{171}\text{Yb}) \left(\frac{f_{170}}{1-f_{170}} \right) \right] \quad (6)$$

$$\times \left\{ \frac{\sigma(^{170}\text{Yb})}{\sigma(^{170}\text{Tm})} + \zeta(^{170}\text{Yb}) \left[\frac{1}{1-f_{170}} + \frac{1}{\tau_o \sigma(^{170}\text{Tm})} \right] f_{170} \right\}^{-1} \frac{\sigma N^\circ(^{170}\text{Yb})}{\sigma N^\circ(^{176}\text{Lu})} .$$

In this expression, f_{170} and f_{171} are the fractions of the time that ^{170}Tm and ^{171}Tm (respectively) emit an electron relative to capturing a neutron; f_n is the neutron-capture branching ratio at ^{176}Lu ; τ_o is the usual parameter characterizing the exponential exposure distribution; and the quantities $\zeta(AZ)$ are defined as:

$$\zeta(AZ) \equiv \left[1 + \frac{1}{\tau_o \sigma(AZ)} \right]^{-1} \quad (7)$$

The rather complicated form of equation (6) can be conveniently examined in two limiting cases. If $f_{170} \rightarrow 1$, then we find that:

$$\frac{N^*(^{176}\text{Lu})}{N^\circ(^{176}\text{Lu})} \rightarrow \left[\frac{1}{f_n} + \frac{1}{\tau_o \sigma(^{176}\text{Lu})} \right]^{-1} \prod_{i=^{171}\text{Yb}}^{^{175}\text{Lu}} \zeta(i) \frac{\sigma N^\circ(^{170}\text{Yb})}{\sigma N^\circ(^{176}\text{Lu})} , \quad (8),$$

which is of course independent of f_{171} as it should be since $f_{170} \rightarrow 1$ merely corresponds to the usual unbranched path with all of the neutron current passing directly through ^{170}Yb . In the other extreme where $f_{170} \rightarrow 0$, we find that equation (6) becomes

$$\frac{N^*(^{176}\text{Lu})}{N^\circ(^{176}\text{Lu})} \rightarrow \left[\frac{1}{f_n} + \frac{1}{\tau_o \sigma(^{176}\text{Lu})} \right]^{-1} \prod_{i=^{172}\text{Yb}}^{^{175}\text{Lu}} \zeta(i) \left[1 + \frac{1-f_{171}}{\tau_o \sigma(^{171}\text{Tm})} \right]^{-1} \\ \{ 1+f_{171} [\zeta(^{171}\text{Yb})-1] \} \frac{\sigma(^{170}\text{Tm})}{\sigma(^{170}\text{Yb})} \frac{\sigma N^\circ(^{170}\text{Yb})}{\sigma N^\circ(^{176}\text{Lu})} \quad (9),$$

where the effect of the cross-section ratio $\sigma(^{170}\text{Tm})/\sigma(^{170}\text{Yb})$ is the most pronounced since the amount of ^{170}Yb that we observe today would have been produced entirely as ^{170}Tm in the limit $f_{170} \rightarrow 0$. One should also notice from the form of equation (9) that changes in the ratio caused by allowing f_{171} to vary from 0 to 1 are much less noticeable than those caused by changing f_{170} .

In principle, f_{170} and f_{171} could both be functions not only of the free-neutron density through the neutron-capture rates but also of the stellar temperature if the effects of excited-state beta decays are important. (Note that if all capture cross sections scale with temperature as $T^{-1/2}$, then the neutron-capture rates are functions only of the free-neutron density.) However, since the ground-state β^- decays of ^{170}Tm and ^{171}Tm are both first-forbidden transitions, examination of their low-lying excited states (Lederer and Shirley 1978) shows that none have any less-forbidden β^- decays so that it is unlikely that any thermal enhancements (Ward, Newman, and Clayton 1976) of these ground-state decays would appreciably reduce their (already short) laboratory half-lives. Therefore, we may assume f_{170} and f_{171} to be dependent only on the free-neutron density.

The major assumption in our development of equation (6) is that the mean s-process neutron exposure is continuous in time. Ward and Newman (1978) have discussed the general modifications to such a formulation caused by a repeated pulsed s-process neutron flux in which ^{170}Tm and ^{171}Tm can freely decay during the long neutron-free periods between pulses. They showed that the continuous-exposure limit (for which equation |6| is valid) is obtained whenever the time required for ^{170}Tm to capture a neutron is much shorter than the duration of a typical pulse. In particular, we see that the half-life of ^{170}Tm against neutron capture is $t_n(^{170}\text{Tm}) = 4.1 \times 10^7/n(\text{cm}^{-3})$ years, so that our formulation of equation (6) will still be valid in a pulsed s-process environment as long as the pulse duration, Δt , and the average neutron density satisfy both sides of the relation:

$$\Delta t \gg 4.1 \times 10^7/n(\text{cm}^{-3}) \sim 0.35 \text{ years.} \quad (10)$$

However, if large free-neutron densities conspire with short exposure times to violate (10), then a model-dependent calculation becomes necessary. Since we are not promoting any particular stellar s-process model, we will not pursue this point further in this section except to point out that the general

effect of a pulsed s-process exposure would be to restore the σN -value of ^{170}Yb to its unbranched level (Ward and Newman 1978) due to the fact that ^{170}Tm in such an environment would not have enough time to capture a neutron during a pulse before decaying to ^{170}Yb between pulses. Thus, our limiting expressions (8) and (9) effectively bracket the entire range of effects of branching at ^{170}Tm and ^{171}Tm .

We also note that the foregoing formulation of the effects of s-process branching for the synthesis of ^{170}Yb can be applied equally well to the situation at s-only ^{160}Dy . If one attempts to extrapolate s-process yields from ^{160}Dy out to ^{176}Lu , care must be taken that the observed abundance today of ^{160}Dy could be influenced in exactly the same way by neutron capture on the odd-odd isotope ^{160}Tb ($t_{1/2} = 72$ days) which has the very large (Holmes et al. 1976) cross section of $\sigma(^{160}\text{Tb}) = 3230$ mb. Therefore, to ascertain the effects of branching at $A = 160$, one can simply transcribe our results in equations (6)-(10) with appropriate changes in the species involved.

Before we start to calculate numerically the original stellar abundance of ^{176}Lu according to equation (6), we can examine the limiting case of practically insignificant neutron branching at ^{170}Tm ($f_{170} \rightarrow 1$) using equation (8). The measured cross sections from Beer and Käppeler (1980) and the presently determined values inserted into equation (8) result in the abundance ratio $N^*(^{176}\text{Lu})/N^{\circ}(^{176}\text{Lu}) = 0.89 \pm 0.10$ which cannot be converted into a mean age $\langle T \rangle$ according to equation (3), even if we take into account the various uncertainties of the measured cross sections. Taking this result as evidence for the real existence of branching at ^{170}Tm , we can now proceed in accordance with equation (6). However, this calculation involves not only laboratory measurements of capture cross section supplemented with theoretical values of Holmes et al. (1976) (Table 6), but also requires a well-determined value for the mean neutron density. Various studies (Ulrich 1973; Peterson and Tripp 1973; Blake and Schramm 1975; Ward, Newman, and Clayton 1976; Macklin and Winters 1976) place this number between 10^7 and 10^9 neutrons per cm^3 . Using $\tau_0 = 0.22 \text{ mb}^{-1}$ (Beer and Käppeler 1980) and neutron densities of 10^7 , 4×10^7 , 10^8 , and 10^9 cm^{-3} , the mean age $\langle T \rangle$ for ^{176}Lu would be 0, 11.4, 23.4, and 45.1 billion years, respectively.

In order to get a better assessment of the mean age, we can use ^{148}Sm as a normalization point and extrapolate the resulting σN curve out to ^{176}Lu . ^{148}Sm has a relatively well established capture cross section (Table 6) and a practically insignificant branching effect from ^{148}Pm . The corresponding calculation yields a mean age between 5 and 10 billion years due to a 6% change in the Sm abundance from Cameron (1973) to Cameron (1981).

Another quite different approach to the problem of obtaining a reliable extrapolation via σN systematics to $A = 176$ is to use all s -only nuclei from ^{96}Mo to ^{204}Pb as normalization points and perform a least squares fit to fix the average time integrated neutron flux τ_0 and the number of exposed iron seed. This calculation was carried out by Käppeler *et al.* (1980) with a selected set of cross sections for four available compilations of solar abundances: Cameron (1973), Suess and Zeh (1973), Zeh (1980), and Cameron (1981). The respective values of $\sigma N(176)$ are: 5.36, 5.82, 5.92 and 5.47 mb ($S_i \equiv 10^6$). If we adopt the σN value of the most recent compilation of Cameron (1981) and account for the various uncertainties [for $\sigma N(176)$: 4%, B: 10%, $N^0(^{176}\text{Lu})$: 3%, $\sigma(^{176}\text{Lu})$: 5%], we arrive at an upper limit for the mean age of 11 billion years. With respect to branching at ^{170}Tm , our estimate of the s -process age would then limit the mean neutron density, $\langle n \rangle$, of the s -process to the range: $10^7 \leq \langle n \rangle \leq 4 \times 10^7 \text{ cm}^{-3}$.

Our result for the mean age $\langle T \rangle$ from the ^{176}Lu clock is compared in Table 6 with previous age determinations via the U/Th and the ^{187}Re decay. In spite of the relatively small uncertainties given for the U/Th and $^{187}\text{Re}/\text{Os}$ ages with respect to our result, we do not think that these former determinations are any more reliable.

The first long-lived chronometer investigated was the U/Th clock (Fowler and Hoyle 1960). Since the half-lives of U and Th are comparable to the r -process age to be determined, this clock cannot yield a model independent average age. In the calculation of the original U/Th ratio one must rely strongly on theoretical concepts of the r -process for which it appears difficult to estimate the uncertainty. There might also be some possibly overlooked effects such as beta delayed fission (Wene 1975)

and the shape of the beta strength function (Klapdor and Wene 1979). In addition, the U/Th solar abundance ratio seems to be subject to large changes (for instance 30% from Cameron 1973 to Cameron 1981). Considering all these arguments, we believe that the uncertainty of the U/Th age of $(7 \pm 2) \times 10^9$ yr (Fowler and Hoyle 1960) is underestimated.

The ^{187}Re -decay has a beta endpoint energy of only 2.6 keV so that, for example, electron capture from excited levels in ^{187}Os back to ^{187}Re is possible. Another effect which has been discussed (Clayton 1969; Perrone 1971; Hiergeist 1976; Conrad and Zeh 1978) is the enhancement of the ^{187}Re decay into bound electron states in ^{187}Os due to its partial ionization in stellar interiors. Thermal effects are also involved in the capture cross section of ^{187}Os which is needed to determine the radiogenic ^{187}Re . ^{187}Os has an excited level at only 9 keV which can easily be populated in the hot interior of a star, so that part of the neutron capture occurs on this state. This excited state capture cannot be measured, and theoretical calculations yield correction factors which differ by a factor of 1.8 (Winters, Macklin, and Halperin 1980). Due to a possible branching at ^{185}W , \underline{s} -process synthesis could also interfere with the \underline{r} -process at ^{187}Re . As the \underline{s} -process must not necessarily have the same time history, this could alter the \underline{r} -process age. For a $\geq 10\%$ branching of the \underline{s} -process path to ^{186}W and ^{187}Re , a neutron density of $\geq 6 \times 10^7 \text{ cm}^{-3}$ would be required. Although the uncertainty of the mean age determined from $^{187}\text{Re/Os}$ (Winters, Macklin, and Halperin 1980) does not include the uncertainty of the half-life, we still believe that the quoted uncertainty of 1.5 billion years is too optimistic. The influence of thermal effects on the beta-decay of ^{187}Re must be investigated in detail to find out whether it can be regarded as a chronometer at all.

Compared to the above cases, ^{176}Lu offers some important advantages. It has a large well-determined half-life of 36 ± 1.6 billion years. The relatively large beta endpoint energy of 589 keV ensures that the beta decay is not affected thermally. It represents a pure \underline{s} -process chronometer with no interference from the \underline{r} -process, and therefore the \underline{s} -process serves to determine the radiogenic ^{176}Lu . Any \underline{s} -process model dependence in this procedure of extrapolating from a nearby \underline{s} -only nucleus to ^{176}Lu is probably very weak. Lu belongs to the rare earths, which have well-known relative abundances and several \underline{s} -only nuclei from which to calculate the radiogenic ^{176}Lu . All quantities needed for the clock can be determined experimentally. The only difficulty introduced is due to the

isomeric state in ^{176}Lu at 127 keV with its rapid beta decay to ^{176}Hf .

In the present discussion, we have always assumed that this isomeric state is not thermally coupled to the ground state, but this is only true if the temperature at the site of the s-process remains below a certain limit. The conditions for a thermal equilibration of ground and isomeric states are the subject of the next section.

b) Stellar Thermal Equilibration of $^{176}\text{Lu}^o$ and $^{176}\text{Lu}^m$

In this section, we will discuss the various stellar regimes in which the ^{176}Lu decay can be used as either a cosmochronometer of galactic nucleosynthesis or as a stellar thermometer of s-process nucleosynthesis. In Figure 4 we have schematically shown the properties of the first 20 excited states of ^{176}Lu (Lederer and Shirley 1978) that can be of importance for providing intermediate coupling between the ground and isomeric states of ^{176}Lu . The fraction of the stellar (~ 30 keV) neutron captures on the $7/2^+$ ground state of ^{175}Lu that initially populate the long-lived ground state is designated as B, with the remaining fraction $1-B$ following gamma cascades that ultimately lead to $^{176}\text{Lu}^m$ (3.68 hours). These lowest-lying states have also been separated according to their rotational band structure (Balodis et al. 1972; Horen and Harmatz 1976) in order to emphasize the possible importance of K-selection rules (Alaga et al. 1955) in determining interband electromagnetic transition rates. The inhibition factor of $\delta = 10^{-2} |\Delta K|^{-\lambda}$ given in the figure was chosen because of the empirical observation (Löbner 1968) that if $|\Delta K| > \lambda$, then every degree of K-forbiddenness corresponds to a retardation by a factor of ~ 100 relative to that predicted by using theoretical Weisskopf single-particle transition rates.

To ascertain whether or not the ground state and the isomer are in fact able to maintain their separate identities under stellar conditions, we have used the formalism of Ward and Fowler (1980) to integrate numerically the coupled set (in this case 20) of first order differential equations describing the complete time evolution at constant stellar temperature and free-neutron density of the population of each state of ^{176}Lu shown in Figure 4. For simplicity, we have also taken the ground state and the isomer to be fed by a constant $^{175}\text{Lu}(n,\gamma)$ source characterized by the branching ratio B. Furthermore, to model all of the possible electromagnetic links connecting the excited states of ^{176}Lu , we have used Weisskopf single-particle estimates for calculating the internal transition rates from a given level down to each state lying below it in energy. We have had to resort to these theoretical rates since none of the individual transition rates have yet been experimentally measured.

Since the single-particle transition rates are known typically to overestimate the true transition rates in those cases where measurements are available, we have also performed the calculations in which we have systematically decreased all of these theoretical rates by various factors. In particular, for such highly deformed rare-earth nuclei as ^{176}Lu the so-called "K selection rule" can greatly inhibit electromagnetic transitions between various rotational bands unless the angular momentum of the emitted photon is at least as large as the change in the projection of the rotational angular momentum required in going from one band in the nucleus to the other. This effect is especially pronounced in the case of ^{176}Lu since no transitions between the $K = 0$ or 1 bands and the $K = 7$ ground state band are observed in the laboratory. Finally, once all of these downward transition rates are obtained, they are then augmented by the usual stimulated-emission factor, and the corresponding upward transition rates are simply obtained by applying the principle of detailed balance.

For the s-process nucleosynthesis of ^{176}Lu (and ^{176}Hf through the beta-decay of ^{176}Lu), we are interested in the value of the neutron-capture branching ratio, f_n , for the entire nucleus since the amount of ^{176}Lu originally produced in a star is:

$$N^*(^{176}\text{Lu}) = f_n \cdot N(176) \quad , \quad (11)$$

where $N(176)$ is the total s-process yield at atomic weight 176. Note that equation (11) is now the correct generalization of equation (4). If we assume that only $^{176}\text{Lu}^o$ and $^{176}\text{Lu}^m$ are sufficiently long-lived to capture a neutron and/or to beta-decay, then the general form for f_n is given by (Ward and Fowler 1980):

$$f_n = \frac{\lambda_n^o N_o(t \rightarrow \infty) + \lambda_n^m N_m(t \rightarrow \infty)}{(\lambda_n^o + \lambda_\beta^o) N_o(t \rightarrow \infty) + (\lambda_n^m + \lambda_\beta^m) N_m(t \rightarrow \infty)} \quad ; \quad (12)$$

where $\lambda_n^{o,m}$ and $\lambda_\beta^{o,m}$ are the neutron capture and beta-decay rates, respectively, of $^{176}\text{Lu}^o$ and $^{176}\text{Lu}^m$. The abundances $N_o(t \rightarrow \infty)$ and $N_m(t \rightarrow \infty)$ of each state are obtained at a given fixed stellar temperature and neutron density by integrating numerically the coupled differential equations

until a steady state is achieved. Here, we are implicitly assuming that the temperature and the neutron density remain reasonably constant for times longer than any neutron capture or beta-decay time scales. The quantitative changes caused by the "freezing-out" of the temperature and the neutron density at the termination of an s-process event will be discussed later in §IV. However, before discussing the general results of the procedure described above, we must briefly discuss two very important limiting cases of equation (12).

In the limit that coupling between the ground state and the isomer via higher-lying levels is ineffective compared to external nuclear destruction by neutron capture and/or beta-decay, we find that:

$$f_n \rightarrow B \left(1 + \frac{\lambda_\beta^o}{\lambda_n^o}\right)^{-1} + (1-B) \left(1 + \frac{\lambda_\beta^m}{\lambda_n^m}\right)^{-1} \quad (13)$$

$$= B \left(1 + 1.48 \times 10^{-3}/n\right)^{-1} + (1-B) \left(1 + 1.27 \times 10^{11}/n\right)^{-1}$$

$$\approx B \text{ only if } \lambda_n^o \gg \lambda_\beta^o \text{ and } \lambda_n^m \ll \lambda_\beta^m,$$

where the explicit numerical results shown above were obtained by taking $\sigma(^{176}\text{Lu}^m) = \sigma(^{176}\text{Lu}^o) = 1718 (3.48/T_8)^{1/2} \text{mb}$ (ie., merely normalized to its value at 30 keV with a simple $T^{-1/2}$ temperature dependence). Furthermore, the stellar temperature, T_8 , will be measured in units of 10^8 K and the stellar neutron density n , in cm^{-3} . From equation (13) we see that equation (11) reduces to equation (4), ie. $f_n = B$, only if $n \ll 1.27 \times 10^{11} \text{cm}^{-3}$; otherwise, neutron capture can begin to compete with the 3.68 hour beta-decay of $^{176}\text{Lu}^m$.

In the opposite extreme where the internal electromagnetic links can rapidly achieve at thermal-equilibrium distribution of level populations, we then must have that

$$f_n \rightarrow \frac{\lambda_n^o + \frac{(2J_m + 1)}{(2J_o + 1)} \exp(-\epsilon_m/kT) \lambda_n^m}{(\lambda_n^o + \lambda_\beta^o) + \frac{(2J_m + 1)}{(2J_o + 1)} \exp(-\epsilon_m/kT) (\lambda_n^m + \lambda_\beta^m)} \quad (14)$$

$$\sim \left[1 + \frac{1}{5} \exp(-14.74/T_8) (1 + 1.27 \times 10^{11}/n) \right]^{-1} \text{ for } T_8 < 10 ,$$

where we have completely neglected the very slow beta-decay of the ground state relative to its rate for capturing neutrons.

From the limiting forms displayed above in equations (13) and (14), it is clear that two distinct regimes exist for the stellar nucleosynthesis of ^{176}Lu . Firstly, for sufficiently low temperatures, the condition of weak internal coupling given by equation (13) allows the laboratory measurement of the branching ratio B to be used directly as a chronometer of galactic s-process nucleosynthesis (see the discussion in §IIIa) in conjunction with the total theoretical s-process yield at $A = 176$ and the measured cross section and abundance of ^{176}Lu as shown in equation (4). Secondly, as the stellar temperature increases, the limit of rapid internal thermal equilibration by the surrounding bath of hot stellar photons as expressed in equation (14) implies that the entire ^{176}Lu has "forgotten" the initial fractions in which $^{176}\text{Lu}^o$ and $^{176}\text{Lu}^m$ were formed. Therefore, the resulting rapid competition between neutron capture and the thermally-enhanced beta-decay of $^{176}\text{Lu} \rightarrow ^{176}\text{Hf}$ constitutes a stellar s-process thermometer. As discussed by Ward (1977) and by Ward and Newman (1978), the disadvantage of this latter situation results from its potentially extreme temperature dependence on the details of s-process "freezing"—ie., the relative rates at which the temperature and the neutron density decrease following an s-process event. If we use the s-process abundance yields at $A = 176$ to calibrate an s-process thermometer then equations (11) and (14) show that the requisite steady stellar neutron density is related to the prevailing temperature by:

$$T_8 = \frac{14.74}{\ln \left\{ \frac{(1 + 1.27 \times 10^{11}/n)}{5 \left[\frac{N(176)}{N^*(^{176}\text{Lu})} - 1 \right]} \right\}} \quad (15)$$

for $1 \leq T_8 \leq 10$.

In Figures 5a and 5b we have plotted the temperature dependence of the steady-state branching ratio f_n given by equation (12) as a function

of the stellar temperature T_8 for the fixed neutron densities: $n = 10^7 \text{ cm}^{-3}$ and $n = 10^9 \text{ cm}^{-3}$, respectively. These two values for the mean s-process neutron density were chosen in order to bracket typical values obtained in studies of s-process branching through the solar system's heavy elements (Ulrich 1973; Peterson and Tripp 1973; Blake and Schramm 1975; Ward, Newman, and Clayton 1976; Macklin and Winters 1976). The families of solid curves show how equation (12) evolves from the low-temperature limit of equation (13) into the thermal equilibrium embodied in equation (14) for two initial values of B . Additionally, each curve is labeled with the appropriate value of δ , the systematic scale factor by which all of the internal electromagnetic transition rates are multiplied. Both parts of Figure 5 show the results of numerical integration for the two different initial conditions: $B = 0.01$ and 0.36 . The thermal-equilibrium values for f_n are shown by the dashed curves in both parts of Figure 5.

The general behavior of the curves in Figure 5 quantitatively verify our expectations that decreasing δ and/or decreasing B both result in a delay in the onset of internal thermal equilibrium. However, in order to understand why order-of-magnitude changes in B and δ result in only relatively modest changes in the stellar temperature at which the internal electromagnetic links begin to thermally equilibrate $^{176}\text{Lu}^o$ and $^{176}\text{Lu}^m$, we must examine the internal equilibration process in a little more detail.

As is the case for all such long-lived isomeric states, the direct electromagnetic transition from $^{176}\text{Lu}^m$ down to $^{176}\text{Lu}^o$ is too slow (even when augmented by stimulated emission by the hot stellar photon bath) to compete effectively with the isomer's fast 3.68 hour beta-decay to ^{176}Hf . Therefore the internal links needed to connect $^{176}\text{Lu}^m$ and $^{176}\text{Lu}^o$ must be indirectly established via intermediate higher-lying excited states (Ward and Fowler 1980). Although, in general, we expect such a transition actually to be mediated by an entire ensemble of excited states (that also couple with each other as well as with $^{176}\text{Lu}^m$ and $^{176}\text{Lu}^o$), at sufficiently low stellar temperatures one can often isolate a single intermediate state as being the most effective link in a given temperature range. This effect is most easily seen from the work of Ward and Fowler (1980) in which they showed that if $^{176}\text{Lu}^o$ and $^{176}\text{Lu}^m$ (specializing their general results to

the case at hand) are to communicate with each other via a single intermediate state, i , then the rapid establishment of thermal equilibrium at a given temperature T requires that both of the following conditions be satisfied:

$$\frac{g_i}{15} \frac{f_{i0} f_{im} \delta \lambda_i}{(1-B)} \exp(-\epsilon_i/kT) \gg \lambda_n^o + \lambda_\beta^o \approx \lambda_n^o \quad (17)$$

and

$$\frac{g_i}{3} \frac{f_{i0} f_{im} \delta \lambda_i}{B} \exp [-(\epsilon_i - \epsilon_m)/kT] \gg \lambda_n^m + \lambda_\beta^m \approx \lambda_\beta^m \quad (18)$$

In the above equations, λ_i is the total (theoretical) downward electromagnetic decay rate of the intermediate excited state at energy ϵ_i and with statistical factor g_i ; δ is the common scale factor multiplying all theoretical single-particle transition rates; and f_{i0} and f_{im} are the relative fractions of the time that state i decays to $^{176}\text{Lu}^o$ and to $^{176}\text{Lu}^m$, respectively.

Now, if both equations (17) and (18) are satisfied at some particular combination of T , δ , and B , then with all other quantities fixed, the changes $\delta \rightarrow \delta'$ and $B \rightarrow B'$ can be compensated for by a shift in the stellar temperature to:

$$T' = \max \left\{ \frac{T}{1 + \frac{kT}{\epsilon_i} \ln \left[\frac{\delta'}{\delta} \left(\frac{1-B}{1-B'} \right) \right]}, \frac{T}{1 + \frac{kT}{(\epsilon_i - \epsilon_m)} \ln \left(\frac{\delta'}{\delta} \frac{B}{B'} \right)} \right\} \quad (19)$$

Thus, the weak logarithmic dependence of T' on changes in δ and B displayed explicitly in equation (19) shows why the order-of-magnitude changes in δ and B illustrated in Figure 5 cause only modest changes in the temperature at which internal thermal equilibrium is re-established. In Figure 4, the higher-lying intermediate states that are the most effective at low temperatures in linking indirectly the ground state and the isomer are indicated by the thicker horizontal lines and italics.

One might think that also merely by increasing the stellar neutron density and thereby increasing the external destruction rates of $^{176}\text{Lu}^o$ and $^{176}\text{Lu}^m$ that the attainment of thermal equilibrium could perhaps be postponed until even higher temperatures are reached. This would then seem to prolong the use of a laboratory measurement of B as a direct s-process chronometer. Unfortunately, as shown by the $B = 0.01$ curves in Figure 5b, this is complicated by the fact that neutron capture on $^{176}\text{Lu}^m$ can begin to

compete with its beta decay and thereby cause the effective value of f_n to increase beyond B even for low temperatures where thermal equilibrium is not achieved. Although this effect is not so dramatic for larger values of B (see the $B = 0.36$ curve in Figure 5b), if one advocates a mean s-process neutron density as high as $n = 10^{11} \text{ cm}^{-3}$, then even for $B = 0.36$, equation (13) shows that for no thermal equilibrium:

$$f_n = 0.36 + \frac{0.64}{1+1.27} = 0.64 \quad . \quad (20)$$

An additional point to note carefully from Figure 5 is that even in those temperature regimes where thermal equilibrium is attained, the experimental determination of B is still an important quantity for s-process nucleosynthesis! This is especially apparent had the value of B proven to be as small as 0.01 as shown in Figure 5a. For the relatively low neutron density shown there, we see that for $\delta < 10^{-6}$, an s-process characterized by $n = 10^7 \text{ cm}^{-3}$ could not have made a major contribution to forming the solar-system material since $f_n < N^\circ(^{176}\text{Lu})/N(176)$ for all T_8 if $\delta < 10^{-6}$. Physically, this interesting constraint merely results from the fact that with such a combination of n and δ , the temperature at which internal thermal equilibrium is finally reached is sufficiently high that the thermal value for f_n is decreasing very rapidly and has already fallen below $N^\circ(^{176}\text{Lu})/N(176)$. Thus, our laboratory determination of B can also serve to place lower limits on the allowed values of n and δ that can yield: $f_n \geq N^\circ(^{176}\text{Lu})/N(176)$ for some T_8 .

In Table 7 we have summarized the various regimes of stellar temperature in which the decay $^{176}\text{Lu} \rightarrow ^{176}\text{Hf}$ can be used as either a cosmochronometer of galactic s-process nucleosynthesis or as a thermometer of s-processing stellar interiors. For definiteness we have taken our measured value of $B = 0.36$ at 24 keV in compiling the table [note that for thermal neutrons, we also have that $B(0.025 \text{ eV}) = 0.36$]. Since the results are virtually independent of the stellar free-neutron density, we have tabulated the boundaries for several values of δ . In the intermediate regions between these temperature extrema, the full network of differential equations coupling all of the excited states of ^{176}Lu must be used to follow the individual fates of $^{176}\text{Lu}^o$ and $^{176}\text{Lu}^m$.

The major conclusion to be drawn from the preceding results is that, in general, the wide variety of spins and parities of the higher-lying excited states of ^{176}Lu afford a fairly efficient means of indirectly equilibrating the populations of $^{176}\text{Lu}^o$ and $^{176}\text{Lu}^m$. In fact, even using our most pessimistic opinion of the theoretical Weisskopf single-particle rates with $\delta = 10^{-8}$, it appears that direct laboratory measurements of $B = 0.36$ can be used in s-process cosmochronologies only if the s-process in nature occurs at stellar temperatures $\leq 1.9 \times 10^8$ K. The effects on this limit of varying δ can be ascertained from Table 7.

Finally, we would like to point out that under the conditions of rapid internal thermal equilibrium, the stellar temperature during neutron-free periods must not be so high that it "burns out" any freshly-synthesized ^{176}Lu . Because of the rapid beta-decay of the isomeric state, the effective half-life of an entire, thermally-equilibrated ^{176}Lu nucleus is only:

$$t_{1/2}(^{176}\text{Lu}) = \left[\lambda_{\beta}^o + \frac{1}{5} \lambda_{\beta}^m \exp(-\epsilon_m/kT) \right]^{-1} \ln 2 \quad (21)$$

$$\approx 18.5 \exp(14.74/T_8) \text{ hours}$$

in the absence of any neutrons and for $1 \leq T_8 \leq 10$. To illustrate this extreme effect, we have constructed Figure 6. The curves show the variation of the total ^{176}Lu abundance as a function of the time spent in a neutron-free environment for various constant stellar temperatures. The calculations were all started from the initial conditions: $^{176}\text{Lu}(t=0) = B = 0.36$ and $^{176}\text{Lu}^m(t=0) = 1-B = 0.64$, and the internal scaling factor was fixed at $\delta = 10^{-6}$ to allow for the K-forbiddenness of many internal transitions. The curves for $T_8 = 5, 3,$ and 2.5 are virtually identical to the corresponding thermal-equilibrium curves at these high temperatures. However, as the temperature is lowered, the curves evolve as shown toward the curve labelled $T_8 \leq 1.4$, which is the limiting case of low temperatures when there is no efficient coupling between $^{176}\text{Lu}^o$ and $^{176}\text{Lu}^m$ for time scales $\leq 10^4$ years. This asymptotic case evolves very quickly ($t \geq 2 \times 10^{-3}$ y) to its constant value of $B = 0.36$ due to the rapid 3.68 hour beta-decay of the isomeric state. As can be seen from the results in Figure 6, the fact that ^{176}Lu does exist in the solar system can place rather severe constraints on the time that a typical ^{176}Lu nucleus can spend in a high-temperature stellar s-process environment in the absence of any synthesizing stellar neutrons.

c) Problems and Uncertainties

In the previous discussion, the variety of different problems - both experimental and theoretical - involved with the study of ^{176}Lu were elucidated. In this section we will briefly summarize the still-outstanding problems:

- (i) Normalization points for the ^{176}Lu clock. Since two nuclei are needed for a chronology, one must be especially careful about choosing the second member of the pair so that it is not influenced by s -process branching. As was already pointed out in §IIIa, this renders not only ^{170}Yb as unreliable, but also the next lighter s -only nucleus, ^{160}Dy . Apparently, only ^{148}Sm , ^{150}Sm , and ^{176}Hf are free of this additional uncertainty in the mass region $140 < A < 190$ where the σ_N curve is fairly flat. From the standpoint of nuclear properties, ^{176}Hf would obviously be the best chronometric partner for ^{176}Lu since it is the direct beta-decay product. However, since Hf is a member of the group of first transition metals and is not a rare earth like Lu, the two elements differ in their chemical fractionation properties and hence the solar Hf/Lu ratio is not well known, and in this respect the rare-earth isotopes $^{148,150}\text{Sm}$ would be favored. However, even among the rare earths, relative abundances often change from one compilation to the other by 6 to 8%. Nevertheless, it would appear that $^{148,150}\text{Sm}$ are the most preferable normalization points for the ^{176}Lu clock;
- (ii) The fraction, B , of ^{176}Lu that is synthesized directly in the long-lived ground state by neutron capture on ^{175}Lu . This factor is still not known to better than 10%, and since it enters sensitively in all calculations, its neutron energy dependence (which certainly is different from the normal $1/v$ scaling) should also be investigated;
- (iii) The internal decay scheme of ^{176}Lu . The decay properties of the lowest-lying excited states - including interband (no matter how small!) and intraband electromagnetic transitions - are needed to study accurately the internal thermal equilibration of the ^{176}Lu ground and isomeric states. Additional uncertainties are present concerning the excitation energy of the isomeric state (and therefore all $K = 0$ and 1 rotational bands) relative to the ground state. Formerly, the isomer was placed at 290 keV (Lederer, Hollander, and Perlman 1967) but now, due to one

more recent measurement (Prodi et al., 1969), it is believed to lie at only 126.5 keV. In view of the $\exp(-\epsilon/kT)$ dependence of all rates involving this state, we think it worthwhile to confirm this result by a second measurement;

- (iv) The half-life of the ground state of ^{176}Lu . In the latest evaluation of Nuclear Data Sheets, the half-life of $^{176}\text{Lu}^0$ appeared to be well-determined as $(3.6 \pm 0.16) \times 10^{10}$ years. However, a new measurement recently reported by Norman (1980) yielded a value of $(4.08 \pm 0.24) \times 10^{10}$ years - unfortunately, with a relatively large uncertainty.

Although the above points outline the uncertainties in the input nuclear physics of the problem, the detailed time dependence of the s-process temperature and neutron density in various stellar models can also introduce very important additional uncertainties regarding the s-process yields of ^{170}Yb , ^{176}Lu , and ^{176}Hf that emerge from such models.

IV. APPLICATIONS TO A SPECIFIC STELLAR MODEL

As was just discussed, the rapid establishment of thermal equilibrium between $^{176}\text{Lu}^o$ and $^{176}\text{Lu}^m$ can place rather severe constraints on any stellar environments than can produce the currently-observed amount of ^{176}Lu that is present in the solar system because of the extreme temperature sensitivity of the thermally-mixed ^{176}Lu beta-decay rate. In §IIIb we discussed these effects under the simplifying assumptions of both a constant stellar temperature and neutron density. However, in a realistic model for the site of the s-process, one must actually follow the detailed time dependence of $n(t)$ and $T(t)$ during and after the neutron irradiation in order to follow the important "freeze-out" of the neutron-capture and beta-decay rates. Of course, during this process one must also follow all of the internal electromagnetic links in ^{176}Lu to calculate the time dependence of the coupling rates between $^{176}\text{Lu}^o$ and $^{176}\text{Lu}^m$.

As a concrete illustration of the basic technique involved, we have used the helium shell-flashing stars modelled by Iben (1977) as a likely scenario where s-process neutrons are provided by the reaction $^{22}\text{Ne}(\alpha, n)^{25}\text{Mg}$ during the convective phase of the unstable region between the hydrogen- and the helium-burning shells. In Figure 7 we have shown the time dependence of the temperature at the base of the convective shell before, during, and after a typical thermal pulse in a $7-M_{\odot}$ star with a carbon-oxygen core of $1.16-M_{\odot}$. The peak temperature at the base of the shell is 3.74×10^8 K; the convective shell phase lasts ~ 2.6 years following temperature maximum; the time between pulses is ~ 470 years; and the temperature at the base of the shell during the quiescent interpulse period is $\sim 1.60 \times 10^8$ K. Furthermore, following the work of Cosner, Iben, and Truran (1980) we have also shown in Figure 7 the time dependence of the free-neutron density, $n(\text{cm}^{-3})$, for this particular model as:

$$n(t') = 2.4 \times 10^{11} \exp\{-t'/1.78 \times 10^7 - 3.18 [1 - \exp(-t'/1.78 \times 10^7)]\} \text{ cm}^{-3}, \quad (22)$$

where t' is measured from the time of the temperature peak at the base of the convective shell, i.e. $t' = (t-13) \times 10^6$ seconds. Both T_{Base} and n are measured by the left-hand scales in Figure 7. Using this particular model,

we also find that the average neutron density is $\langle n \rangle = 1.6 \times 10^{10} \text{ cm}^{-3}$ over the 2.6-year lifetime of the convective shell following the temperature maximum and that the total integrated neutron exposure during the pulse is $\tau = 0.31 \text{ mb}^{-1}$.

We have used these two prescriptions for $T(t)$ and $n(t)$ in a simplified reaction network to calculate the resulting s-process yields of ^{170}Yb , ^{176}Lu , and ^{176}Hf as a function of time. For the production of ^{170}Yb , we have allowed for s-process branching at ^{170}Tm (as discussed in §IIIa) and have assumed a constant source abundance of ^{169}Tm . Similarly, to follow the time evolution of the abundances of ^{176}Lu and ^{176}Hf , we have assumed a constant source abundance of ^{175}Lu but have retained all of the temperature-dependent couplings among the internal excited states of ^{176}Lu (with $B = 0.36$ and $\delta = 10^{-6}$) as was discussed in §IIIb. Therefore, we are able to follow accurately the "freeze-out" of the abundances as the temperature decreases and the neutron density falls to zero.

The additional solid curves in Figure 7 show the results of the detailed numerical integration described above for the species: ^{170}Yb , ^{176}Lu , and ^{176}Hf . These time-dependent σN -values are measured by the right-hand scale relative to the assumed-constant sources. The additional dashed curves show the results, $^{176}\text{Lu}^{\text{eq}}$ and $^{176}\text{Hf}^{\text{eq}}$, that would be obtained if all of the excited states of ^{176}Lu were always in thermal equilibrium with each other. Note that the time axis in Figure 7 changes from a linear to a logarithmic scale at 100×10^6 seconds. From the figure it is clear that during the time that the neutron source is active, the temperature at the base of the convective shell is sufficiently high that thermal equilibrium among the excited states of ^{176}Lu is maintained until the termination of the convective-shell phase. Furthermore, the temperature between pulses is low enough that the internal electromagnetic links partially freeze-out during the long interpulse period and do not allow the abundance of $^{176}\text{Lu}^{\text{o}}$ to be totally depleted by coupling to the fast beta decay of $^{176}\text{Lu}^{\text{m}}$ - as contrasted to the curve for $^{176}\text{Lu}^{\text{eq}}$. After the termination of the pulse, we obtain the "freeze-out" values: $\sigma N(^{176}\text{Lu})/\sigma N(^{175}\text{Lu}) = 0.41$ and $\sigma N(^{176}\text{Hf})/\sigma N(^{175}\text{Lu}) = 0.39$ for $\delta = 10^{-6}$ and $B = 0.36$. However, if internal couplings are neglected, i.e. $\delta \rightarrow 0$, then our numerical integrations instead yield: $\sigma N(^{176}\text{Lu})/\sigma N(^{175}\text{Lu}) = B = 0.36$ and $\sigma N(^{176}\text{Hf})/\sigma N(^{175}\text{Lu}) = 1-B = 0.64$ for times $\geq 60 \times 10^6 \text{ s}$.

For the case of ^{170}Yb , we obtain the "freeze-out" value of $\sigma N(^{170}\text{Yb})/\sigma N(^{169}) = 0.56$. Note that this value lies between the value of unity that would be obtained if ^{170}Tm had always beta-decayed during the pulse and the value of $\sigma(^{170}\text{Yb})/\sigma(^{170}\text{Tm}) = 766/2260 = 0.34$ that would have been obtained if ^{170}Tm had always captured a neutron. This result is in agreement with our simplified general discussion in §IIIa. We can now combine these "freeze-out" ratios to obtain the amount of ^{176}Lu produced in this particular stellar s-process model (normalized to the currently-observed amounts of ^{176}Lu and ^{170}Yb in the solar system) as:

$$\frac{N^*(^{176}\text{Lu})}{N^\circ(^{176}\text{Lu})} = \left[\frac{\sigma N^*(^{176}\text{Lu})}{\sigma N^*(175)} \right] \left[\begin{array}{c} 175 \\ \Pi \quad \zeta(i) \\ i=170 \end{array} \right] \left[\frac{\sigma N^*(^{170}\text{Yb})}{\sigma N^*(169)} \right]^{-1} \frac{\sigma N^\circ(^{170}\text{Yb})}{\sigma N^\circ(^{176}\text{Lu})}, \quad (23)$$

where we have followed the formalism of §IIIa and the second term in brackets accounts for the (small) decrease in slope of the theoretical σN -curve from $A = 170$ to $A = 175$. The numerical values for the first and third terms in brackets above are strongly dependent upon the particular stellar model as illustrated in Figure 7, and the resulting ^{176}Lu age of s-process material ejected from such a star can then be obtained from equations (23) and (3). Of course, as was pointed out by Cosner, Iben, and Truran (1980), the s-process abundances so calculated would be shell abundances immediately after nucleosynthesis without allowing for mixing with the outer envelope. If several convectively-mixed mass zones were actually involved in the synthesis, then we would need temperature and neutron-density profiles, $T_m(t)$ and $n_m(t)$, for each mass co-ordinate that is participating in the s-processing. The final step would then be to average over the "freeze-out" abundances of each mass zone to obtain the total yield of a given nucleus.

This approach would be a type of mass-averaged convection that has also been discussed by Woosley and Weaver (1980) in their treatment of the stellar synthesis of ^{26}Al . They pointed out that the effects of time-dependent convection can also be important as a radioactive nucleus convectively diffuses (in the absence of any production mechanisms) through the stellar temperature gradient necessary for its abundance to be communicated to the outer envelope. Although their discussion was for the particular case of ^{26}Al , it clearly applies to any nucleus with a long-lived ground state and a much shorter-lived isomeric state, so that thermal equilibrium between the two

would make the overall beta-decay rate a very sensitive function of the stellar temperature. In these special cases one may well need to retain all of the internal electromagnetic couplings among the excited states and follow the time history of the temperature gradient experienced by a "typical" ^{176}Lu nucleus as it convectively diffuses outward from the synthesizing intershell region through one pressure scale height to the outer envelope. Note that this type of a treatment would also in principle apply to the s-process synthesis of the nuclei: ^{87}Rb , ^{113}Cd , ^{115}In , and ^{187}Re - in addition to ^{176}Lu . However, in the absence of any such published mixing profiles, we present the calculations in Figure 7 as a reasonable representation of s-process yield at $A = 170$ and $A = 176$ that would be obtained from applying our general techniques in §IIIa and §IIIb to recent stellar models (Iben 1977; Cosner, Iben and Truran 1980).

V. CONCLUSIONS

In the present investigation we have pointed out that the stellar s-process nucleosynthesis of ^{176}Lu is a much richer problem in both nuclear physics and stellar modelling than was previously thought to be the case. We have attempted to discuss and quantify all of the various interrelated aspects of this problem in a realistic way and to use as much experimental information as possible in analyzing the dual role of ^{176}Lu as both a cosmic clock and a stellar s-process thermometer.

We have shown that thermalization effects in s-process nucleosynthesis cannot be dealt with in a global way since they depend strongly on the individual nuclear properties of each nucleus. In this respect, we must conclude with a warning that the cavalier treatment of the stellar thermalization (or lack thereof) of such nuclear isomeric states must be avoided. In fact, we have explicitly shown that there is a delicate interplay between the internal electromagnetic transitions linking $^{176}\text{Lu}^o$ and $^{176}\text{Lu}^m$ and the time-dependent way in which the stellar s-process temperature and free-neutron density "freeze-out".

We would like to encourage further experimental investigations of ^{176}Lu because, in many ways, the fate of ^{176}Lu is strongly dependent on the size of various nuclear quantities. In our opinion, ^{176}Lu is one of the outstanding nuclei which can act as a test for stellar s-process models in reproducing the amount of ^{176}Lu we observe in the solar system today.

ACKNOWLEDGEMENT

We would like to thank D. Roller for his strong support in providing the neutron beam. We are also indebted to G. Rupp for his continuous help with the experimental set-up.

References

- Alaga, G., Alder, K., Bohr, A., and Mottelson, B. 1955, Dan. Mat. Fys. Medd., 29, no. 9.
- Allen, B.J., and Cohen, B.B. 1979, Aust. J. Phys., 32, 447.
- Arnould, M. 1973, Astron. and Astrophys. 22, 311.
- Audouze, J., Fowler, W.A., and Schramm, D.N. 1972, Nature, 238, 8.
- Balodis, M.K., Tambergs, J.J., Alksnis, K.J., Prokofiev, P.T., Vonach, W.G., Vonach, H.K., Koch, H.R., Gruber, U., Maier, B.P.K., and Schult, O.W.B. 1972, Nucl. Phys., A197, 305.
- Beer, H., and Käppeler, F. 1980, Phys. Rev., C21, 534.
- Beer, H., Käppeler, F., and Wisshak, K. 1979, in Conf. on Nucl. Cross Sections for Technology, Knoxville, Tennessee.
- Blake, J.B., and Schramm, D.N. 1975, Ap. J., 197, 615.
- Block, R.C., Slaughter, G.G., Weston, L.W., and Vonderlage 1961, Proc. Symp. on Neutron Time-of-Flight Methods, Saclay, p. 203.
- Cameron, A.G.W. 1973, Space Sci. Rev., 15, 129 .
- _____. 1981, in Nucl. Astrophysics, ed. C.A. Barnes, D.D. Clayton, and D.N. Schramm (Cambridge University Press: Cambridge 1981).
- Clayton, D.D. 1964, Ap. J. 139, 637.
- _____. 1969, Nature 224, 56 .
- Conrad, J.H., and Zeh, H.D. 1978, Z. Naturforsch., 33a, 887.
- Cosner, K., Iben, I., Jr., and Truran, J.W. 1980, Ap. J. Lett., 238, L91.
- Fowler, W.A., and Hoyle, F. 1960, Ann. Phys., 10, 280.
- Fröhner, F.H. 1968, GA-8380 Gulf General Atomic Report.
- _____. 1980, (private communication).
- Hiergeist, G., 1976, Untersuchung des $^{187}\text{Re} \beta^-$ Zerfalls, Diplomarbeit, Physik Department der Technischen Universität München.
- Holmes, J.A., Woosley, S.E., Fowler, W.A., and Zimmermann, B.A. 1976, Atomic Data and Nucl. Data Tables, 18, 305.
- Horen, D.J., and Harmatz, B., 1976, Nuclear Data Sheets, 19, 383.
- Iben, I., Jr. 1977, Ap. J., 217, 788.
- Käppeler F., Beer, H., Clayton, D.D., Macklin, R.L., and Ward, R.A. 1981, in preparation.
- Klapdor, H.V., Wene, C.-O., 1979, Ap. J., 230, L113.
- Konks, V.A., Popov, Yu.P., and Fomin, Yu.I. 1968, Yad. Fiz., 7, 493; (Sov. J. Nucl. Phys., 7, 310).
- Kononov, V.N., Yurlov, B.D., Poletaev, E.D., and Timokhov, V.M. 1978, Yad. Fiz., 27, 10; (Sov. J. Nucl. Phys., 27, 5).

- Lederer, C.M., Hollander, J.M. and Perlman, I. 1967, Table of Isotopes (6th ed.; New York: Wiley).
- Lederer, C.M., and Shirley, V.S. 1978, Table of Isotopes (7th ed.; New York: Wiley).
- Lépine, I.R.D., Douglas, R.A., and Maia, H.A. 1972, Nucl. Phys., A196, 83.
- Löbner, K.E.G. 1968, Phys. Lett., 26B, 369.
- Macklin, R.L., Gibbons, J.H. 1967, Phys. Rev., 159, 1007.
- Macklin, R.L., Gibbons, J.H. and Inada, T. 1963, Nature, 197, 369.
- Macklin, R.L., and Winters, R.R. 1976, Ap. J., 208, 812.
- McCulloch, M.T., De Laeter, J.R., and Rosman, K.J.R. 1976, Earth. Plan. Sci. Lett., 28, 308.
- Moxon, M.C., and Rae, E.R. 1963, Nucl. Instr. and Method, 24, 445.
- Norman, E.B. 1980, Phys. Rev., C21, 1109.
- Peterson, V.L., and Tripp, D.A. 1973, Ap. J., 184, 473.
- Perrone, F. 1971, unpublished Ph.D. thesis, Rice University.
- Prodi, V., Flynn, K.F., and Glendenin, L.E. 1965, Phys. Rev., 188, 1939.
- Schramm, D.N., and Wasserburg, G.J. 1970, Ap. J., 162, 57.
- Shorin, V.S., Gribunin, V.M., Kononov, V.N., and Sidorova, I.I. 1971, Astrofizika, 7, 489.
- Shorin, V.S., Kononov, V.N., Poletaev, E.D. 1974, Yad. Fiz., 19, 5; (Sov. J. Nucl. Phys., 19, 2).
- Storm, E., and Israel, H.I., 1980, Nucl. Data Tables, A7, 565.
- Suess, H.E., and Zeh, H.D. 1973, Ap. and Space Sci., 23, 173.
- Ulrich, R.K. 1973, in Explosive Nucleosynthesis, ed. D.N. Schramm and W.D. Arnett (Austin: University of Texas Press), p. 139.
- Ward, R.A. 1977, Ap. J., 216, 540.
- Ward, R.A., and Fowler, W.A. 1980, Ap. J., 238, 266.
- Ward, R.A., and Newman, M.J. 1978, Ap. J., 219, 195.
- Ward, R.A., Newman, M.J., and Clayton, D.D. 1976, Ap. J. Suppl., 31, 33.
- Wene, C.-O. 1975, Astr. Ap., 44, 233.
- Winters, R.R., Macklin, R.L., and Halperin, J. 1980, Phys. Rev., C21, 563.
- Wisshak, K., and Käppeler, F., 1978, Nucl. Sci. Eng., 66, 363.
_____ 1979, Nucl. Sci. Eng., 69, 39.
- Woosley, S.E., and Weaver, T.A. 1980, Ap. J., 238, 1017.
- Zeh, H.D., 1980, in preparation.

Table 1: Experimental parameters

	RUN I	RUN II
Neutron reaction	${}^7\text{Li}(p,n)$	${}^3\text{H}(p,n)$
Beam current	20 μA	10 μA
Repetition rate	2.5 MHz	2.5 MHz
Pulse width	700 ps	700 ps
Max. proton energy above reaction threshold	20 keV	100 keV
Time resolution	1.2-1.3 ns	1.2-1.3 ns
Flight path	67 mm	69 mm
Neutron energy range	5-90 keV	50-200 keV

Table 2: Sample characteristics

Sample	Chemical composition	Isotopic composition H (%)	Neutron binding energy E_B (keV) ^B	Weight (g)	Thickness (at/b) ⁴ x 10 ⁴	(MS-SS)	K
¹⁷⁰ Yb	Yb ₂ O ₃	(168) 0.02 (170) 78.78 (171) 10.54 (172) 4.85 (173) 2.08 (174) 3.05 (176) 0.68	(168) 6867.2 (170) 6617.2 (171) 8020.9 (172) 6367.3 (173) 7465 (174) 5822.6 (176) 5566.8	1.704	7.467	1.01	0.997
Yb	Yb ₂ O ₃	natural		5.345	23.113	1.03	0.989
Lu	Lu ₂ O ₃	natural	(175) 6293.2 (176) 7072.1	5.294	22.668	1.03	0.989
¹⁹⁷ Au	metallic	-	6512.7	6.666	28.833	1.04	0.989
C	graphite	natural		1.010	71.641	-	-

Table 3: Systematic uncertainties

	${}^7\text{Li}(p,n)$ (%)	${}^3\text{H}(p,n)$ (%)
${}^{197}\text{Au}$ standard	2.5	2.5
Impurity correction for:		
${}^{170}\text{Yb}$	2	2
${}^{175}\text{Lu}$	0.4	0.4
Normalization of the TOF spectra to the same neutron beam intensity	0.3	0.3
Multiple scattering	0.6	0.6
Constant background subtraction for:		
Au	0.14*	0.7 ⁺
${}^{175}\text{Lu}$	0.08*	0.4 ⁺
${}^{170}\text{Yb}$	0.37*	1.9 ⁺
Yb	0.18*	1.1 ⁺
Flight path	0.3	0.3
Effective binding energy for Yb	0.8	0.8

* at 30 keV neutron energy

⁺ at 90 keV neutron energy

Table 4: Average resonance parameters from the statistical model fit

Target nucleus	Strength function $S_\ell \times 10^4$			Radiation width Γ_ℓ (meV)			Average level spacing D_ℓ (eV)			Effective nuclear radius R (fm)	
	$\ell =$	0	1	2	0	1	2	0	1		2
^{170}Yb		2.25	4.44	0.15	37.29	50.85	50	22.6	8	5.4	7.3
^{175}Lu		1.36	0.48	0.72	149.51	22.97	8.8	3.28	1.75	1.29	7.3

Table 5: Maxwellian-averaged capture cross sections $\langle\sigma\rangle$ for ^{170}Yb and ^{176}Lu

kT (keV)	^{170}Yb		^{176}Lu	
	$\langle\sigma\rangle$ (mb)	Uncertainty (%)	$\langle\sigma\rangle$ (mb)	Uncertainty (%)
10	1197		2327	
20	916		1580	
30	766	4	1266	3.4
40	667		1087	
50	597		973	
60	548		897	
70	512		843	
80	486		804	
90	465		775	
100	450		753	

Table 6: Quantities relevant to the ^{176}Lu clock and comparison of mean ages $\langle T \rangle$ derived from various chronometers

A_Z	$\langle \sigma \rangle$ (mb)		Solar abundance $N^{\odot}(A_Z)$ ($\text{Si} \equiv 10^6$)
	present work	other work	
		281+23§	
		258+48	
^{148}Sm		av. 269+21	0.0254** 0.0270++
^{170}Tm		2260*	
^{171}Tm		917*	
^{170}Yb	766+30	790+60+	0.00654** 0.00606++
^{171}Yb		1453+117†	
^{172}Yb		410+34†	
^{173}Yb		865+72†	
^{174}Yb		176+16†	
^{175}Lu	1266+43	1411+107††	
^{176}Lu	1718+85#		0.00108** 0.00105++

* Holmes et al. (1976), + Allen and Cohen (1979), † Shorin, Kononov and Poletaev (1974), # Beer and Käppeler (1980), § Kononov et al. (1978), || Macklin, Gibbons, and Inada (1963), ** Cameron (1973), ++ (Cameron (1981), †† Macklin and Gibbons (1967)

Cosmic clock	Half life (10^9 yr)	Mean age $\langle T \rangle$ (10^9 yr)
^{176}Lu	36 ± 1.6	< 11
$^{187}\text{Re/Os}$	43 ± 20	6.4 ± 1.5§§
U/Th	4.47/14.05	7 ± 2##

§§ Winters, Macklin, and Halperin (1980)

Fowler and Hoyle (1960)

Table 7: Temperature Regimes for the $^{176}\text{Lu} \rightarrow ^{176}\text{Hf}$ Decay

$$B = 0.36$$

n (cm ⁻³)	δ	T ₈	
		Cosmic Clock	Stellar Thermometer
10 ⁷ → 10 ^{10*}	10 ⁻⁴	≲ 1.3	≳ 1.7
	10 ⁻⁶	≲ 1.6	≳ 2.2
	10 ⁻⁸	≲ 1.9	≳ 3.0

* Note that the additional terms in equation (13) of the main text begin to come into play for values of the neutron density $\gtrsim 10^{10} \text{ cm}^{-3}$.

Appendix

Here we numerically tabulate the detailed microscopic cross sections for neutron capture by: natural Yb (Table A1), ^{170}Yb (Table A2), and ^{175}Lu (Table A3). These experimental results for ^{170}Yb and ^{175}Lu were then used in conjunction with equation (2) of the main text to perform numerically the thermonuclear averages displayed in Table 5.

Table A1: Experimental results for the neutron capture cross section of natural Yb

E_n (keV)	\pm	ΔE_n	σ (Yb) (b)	Uncertainty (%)		
				Statistical	Systematic	Total
RUN I						
4.77		0.68	1.473	3.80	3.49	5.16
6.22		0.76	1.069	3.25	3.47	4.75
7.69		0.70	1.011	3.18	3.46	4.70
8.62		0.34	1.029	5.59	3.88	6.81
9.05		0.36	0.964	4.85	3.78	6.15
9.51		0.38	1.041	4.63	3.75	5.96
10.01		0.40	0.942	4.41	3.72	5.77
10.55		0.43	0.912	4.02	3.67	5.44
11.13		0.46	0.793	3.69	3.62	5.17
11.76		0.49	0.763	3.27	3.59	4.85
12.45		0.53	0.810	3.16	3.57	4.77
13.20		0.57	0.761	3.06	3.56	4.69
14.02		0.61	0.736	2.83	3.54	4.53
14.92		0.66	0.741	2.50	3.52	4.32
15.90		0.72	0.715	2.33	3.51	4.21
16.99		0.78	0.644	2.12	3.49	4.08
18.20		0.85	0.639	1.94	3.48	3.98
19.53		0.94	0.664	1.81	3.47	3.92
21.02		1.03	0.648	1.65	3.47	3.84
22.69		1.14	0.641	1.48	3.46	3.76
24.57		1.27	0.5876	1.31	3.46	3.70
26.68		1.42	0.5455	1.19	3.45	3.65
29.08		1.59	0.5118	1.06	3.45	3.61
31.83		1.80	0.4897	0.99	3.45	3.59
34.97		2.04	0.4455	0.94	3.45	3.57
38.61		2.34	0.4211	0.87	3.45	3.56
42.85		2.70	0.4218	0.82	3.45	3.54
47.83		3.15	0.4081	0.76	3.45	3.53
53.73		3.71	0.3912	0.71	3.45	3.52
60.70		4.42	0.3709	0.67	3.44	3.51
69.35		5.32	0.3296	0.65	3.44	3.51
79.84		6.51	0.2754	0.73	3.45	3.52
92.91		8.10	0.2269	1.30	3.46	3.69
RUN II						
30.67		1.84	0.474	4.20	6.69	7.83
34.18		2.14	0.438	3.66	5.84	6.89
38.31		2.51	0.420	3.20	5.1	6.02
43.24		2.98	0.439	2.65	4.17	4.94
49.18		3.57	0.398	2.21	3.92	4.50
56.42		4.35	0.3737	1.85	3.54	4.0
65.39		5.37	0.3420	1.58	3.29	3.65
76.67		6.76	0.2892	1.39	3.15	3.44
91.14		8.68	0.2373	1.27	3.1	3.32
110.14		11.44	0.2068	1.14	3	3.22
135.72		15.54	0.1773	1.06	2.95	3.14
171.46		21.91	0.1419	1.42	3.18	3.48

Table A2: Experimental results for the neutron capture cross section of ^{170}Yb

E_n (keV)	\pm	ΔE_n	$\sigma(^{170}\text{Yb})$ (b)	Uncertainty (%)		
				Statistical	Systematic	Total
5.17		1.15	1.196	5.48	3.91	6.73
7.55		1.19	1.461	4.46	3.94	5.95
10.05		1.30	1.335	3.14	3.92	5.02
12.47		1.08	0.925	3.15	3.92	5.03
14.02		0.61	1.014	4.73	4.21	6.33
14.92		0.66	1.055	3.98	4.12	5.72
15.90		0.72	0.944	3.77	4.12	5.59
16.99		0.78	0.908	3.53	4.10	5.41
18.20		0.85	0.873	3.23	4.05	5.18
19.53		0.94	1.009	2.87	4.02	4.94
21.02		1.03	1.038	2.49	4.0	4.7
22.69		1.14	0.912	2.26	3.96	4.56
24.57		1.27	0.848	1.94	3.95	4.40
26.68		1.42	0.861	1.71	3.94	4.29
29.08		1.59	0.778	1.53	3.93	4.21
31.83		1.80	0.805	1.37	3.92	4.15
34.97		2.04	0.742	1.33	3.92	4.14
38.61		2.34	0.6571	1.22	3.91	4.10
42.85		2.70	0.7260	1.11	3.91	4.07
47.83		3.15	0.6740	1.02	3.91	4.04
53.73		3.71	0.6420	0.96	3.91	4.02
60.79		4.42	0.6142	0.89	3.91	4.0
69.35		5.32	0.5649	0.86	3.91	4.0
79.84		6.51	0.5291	0.94	3.91	4.02
92.91		8.10	0.4444	1.73	3.92	4.29
38.31		2.51	0.676	5.05	7.82	9.31
43.24		2.98	0.688	4.24	6.62	7.86
49.18		3.57	0.609	3.47	5.79	6.75
56.42		4.35	0.608	2.75	4.94	5.65
65.39		5.37	0.563	2.32	4.4	4.98
76.67		6.76	0.518	1.94	4.06	4.5
91.14		8.68	0.4452	1.75	3.87	4.25
110.14		11.44	0.3778	1.57	3.76	4.07
135.75		15.54	0.3206	1.46	3.7	3.98
171.46		21.91	0.2660	1.95	4.08	4.52

Figure Captions

- Figure 1. The various processes of nucleosynthesis that contribute in the mass region from Er to Hf. The s-process path is shown by the solid line and allows for competition between neutron capture and beta-decay at ^{170}Tm , ^{171}Tm , and ^{176}Lu . Possible r-process contributions are indicated by dashed arrows.
- Figure 2. Schematic set up for the capture cross section measurement. An experimental TOF-spectrum for the ^{175}Lu sample and the corresponding background spectrum are given in the insert.
- Figure 3. Experimental results for the present capture cross section measurements in the energy range 5 to 200 keV compared to previous work. Run I and Run II refer to the $^7\text{Li}(p,n)$ and $^3\text{H}(p,n)$ reaction, respectively. The solid line represents a least squares fit of the present data according to the statistical model.
- Figure 4. Level scheme of the first 20 states of ^{176}Lu showing the various neutron-capture and isomeric branchings involved. In addition to giving the energy (in keV), the spin, and the parity of each state, we have also separated them according to their rotational band structure in order to emphasize the inhibition of interband electromagnetic transition rates by the factor $\delta = 10^{-2} |\Delta K|^{-\lambda}$ if the transition requires that $|\Delta K| > \lambda$. The higher-lying excited states that are most effective at low temperatures in mediating transitions between the isomer and the ground state are indicated by the thicker horizontal lines and the italics.
- Figure 5. a). The neutron-capture branching ratio, f_n , as given by equation (12) of the main text as a function of the stellar temperature T_8 for the constant free-neutron density $n = 10^7 \text{ cm}^{-3}$. Each family of three curves emerges from a common value of B as indicated, and they then separate

according to the value of δ (the internal electromagnetic rate scaling factor) with which they are each labeled. The dashed curve gives the value of f_n appropriate to thermal equilibrium, and the additional horizontal dotted line gives the observed present-day value of $N^{\circ}(^{176}\text{Lu})/N(^{176}) = 0.33$.

b). The same presentation as in part a) except for the higher s-process neutron density: $n = 10^9 \text{ cm}^{-3}$.

Figure 6.

The fraction of the original abundance (normalized to unity at $t=0$) of ^{176}Lu remaining after a time t (in years) in the absence of any synthesizing neutron flux. The curves are each labeled with the appropriate fixed stellar temperature and are all calculated with the median value of $\delta = 10^{-6}$. The initial conditions for the numerical integration were taken to be: $^{176}\text{Lu}^{\circ}(t=0) = 0.36$ and $^{176}\text{Lu}^{\text{m}}(t=0) = 0.64$.

Figure 7.

Time-dependent characteristics of the s-processing convective shell of an asymptotic-branch 7- M_{\odot} star with a carbon-oxygen core of $1.16 M_{\odot}$. The left-hand scale measures both the temperature (after Iben 1977) at the base of the convective shell, T_{Base} , in units of 10^8 K and the free-neutron density, $n(\text{cm}^{-3})$, in the shell (after Cosner, Iben, and Truran 1980) beginning at the time ($t \approx 13 \times 10^6$ seconds) when T_{Base} is a maximum. Note the change from a linear to a logarithmic time axis at $t = 100 \times 10^6$ seconds. The additional solid curves (as measured by the right-hand scale) give the resulting time dependence of the relative σN -values of: (i) ^{176}Lu (with $\delta = 10^{-6}$ and $B = 0.36$), (ii) ^{176}Hf , and (iii) ^{170}Yb , all after maximum temperature and neutron density are attained. The additional dashed curves show the relative σN -values, $^{176}\text{Lu}^{\text{eq}}$ and $^{176}\text{Hf}^{\text{eq}}$, that would be obtained if all of the excited states of ^{176}Lu were always in thermal equilibrium with each other.

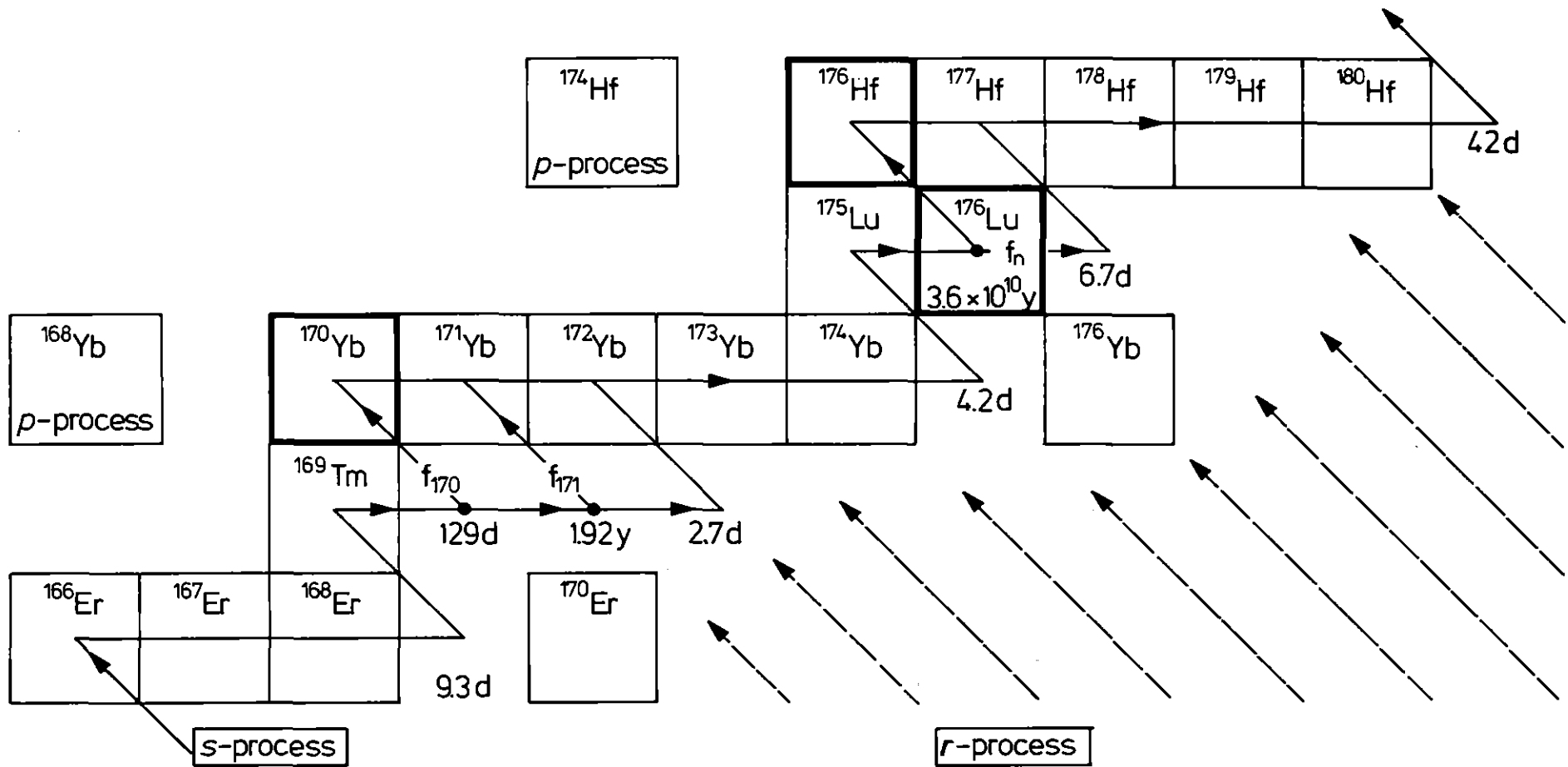
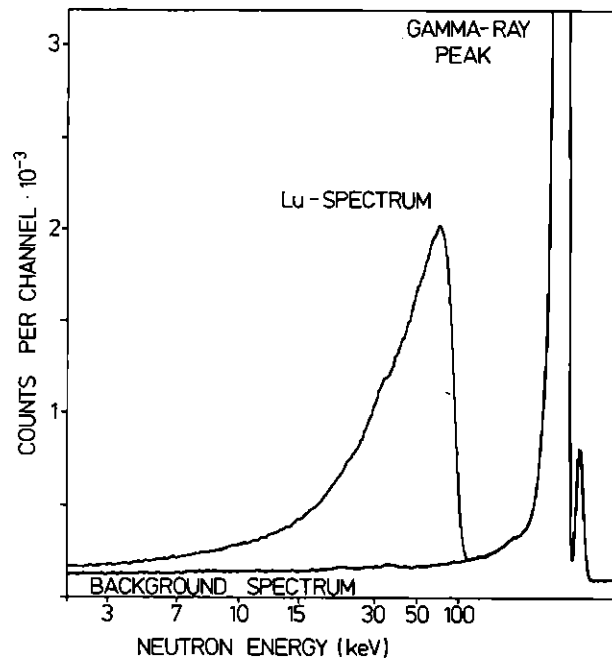
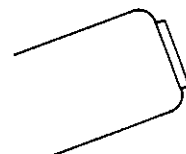


Fig. 1



TRANSMISSION DETECTOR
(at 0 deg, flight path 93.5 cm)



NEUTRON FLUX MONITOR
(at 20 deg, flight path 160cm)

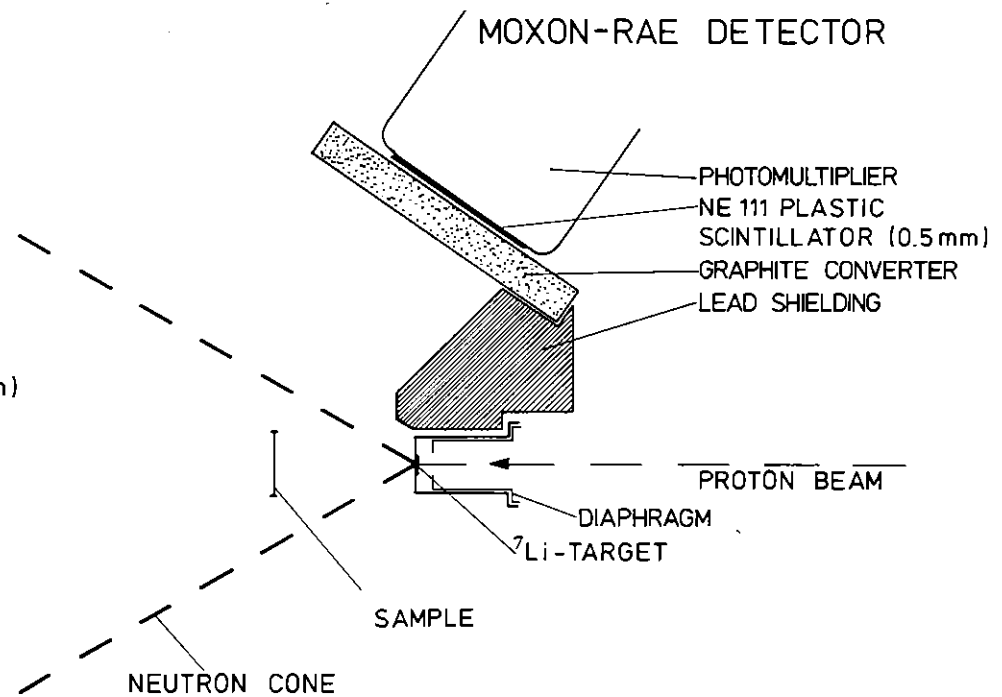


Fig. 2

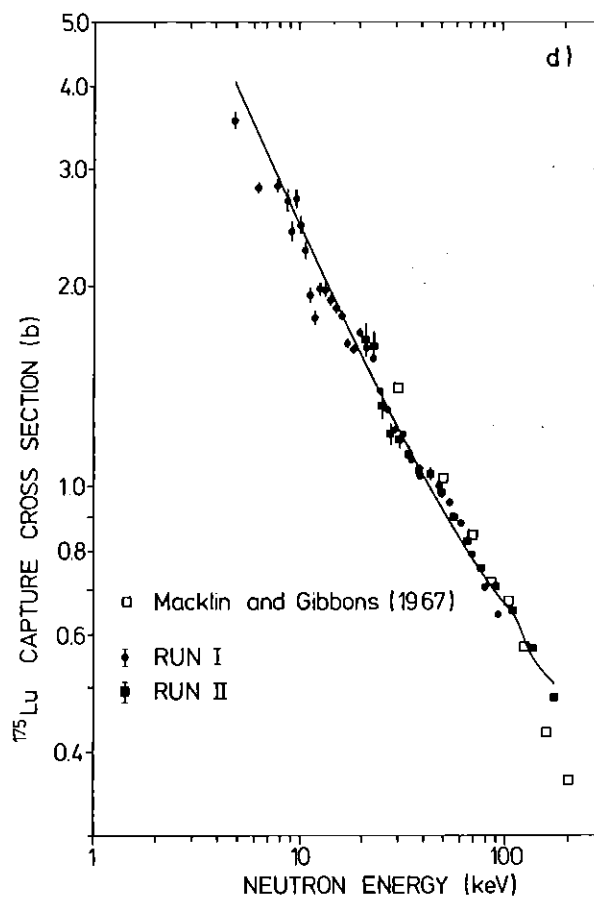
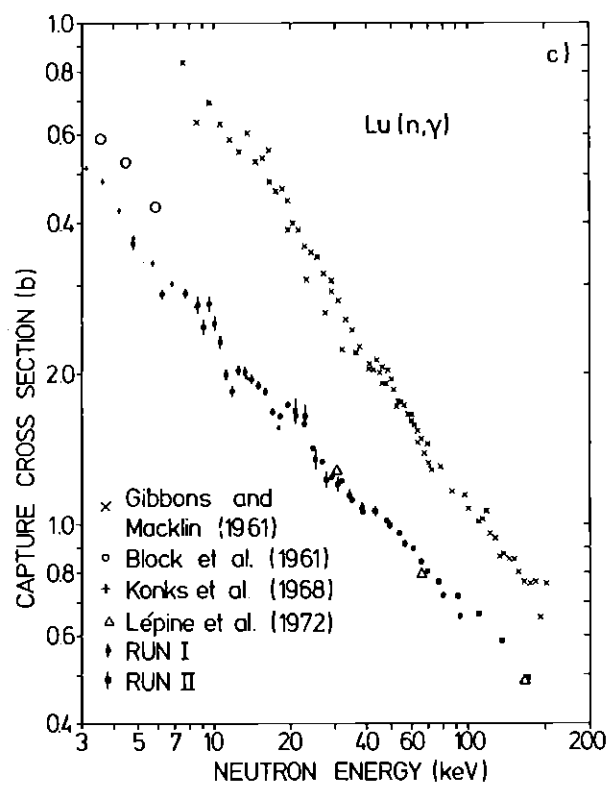
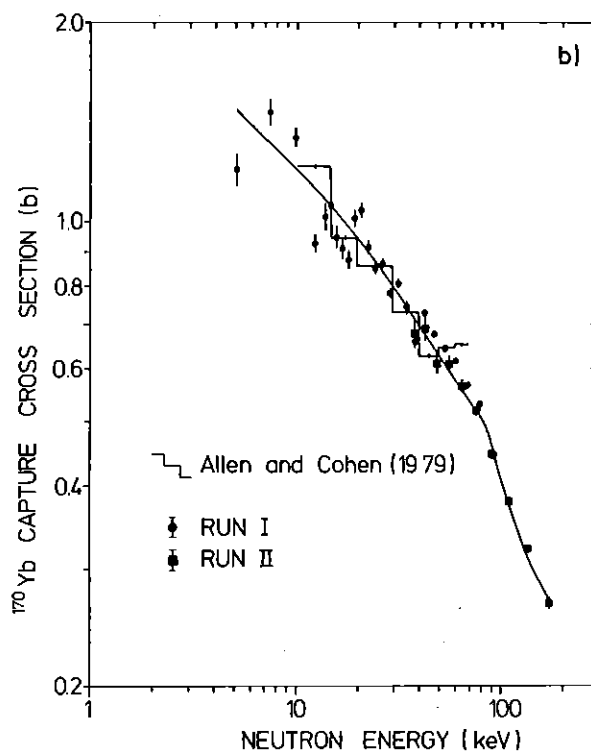
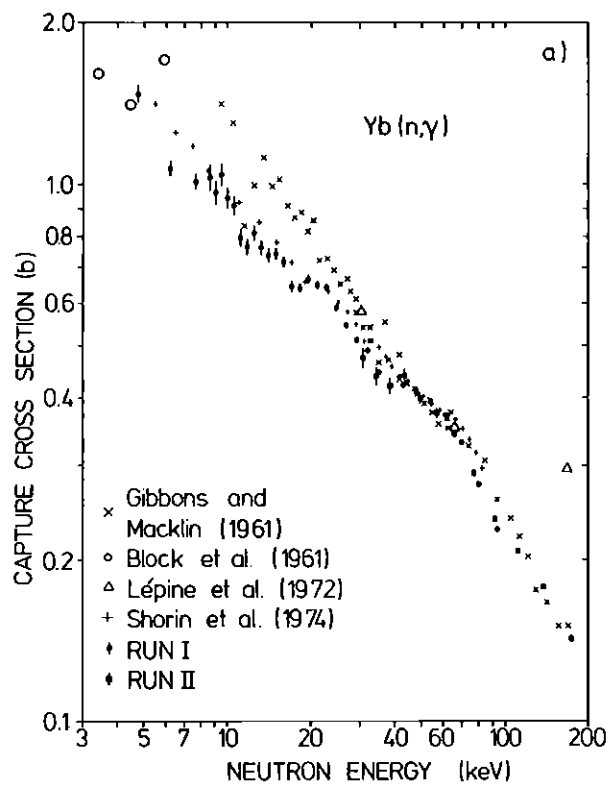


Fig. 3

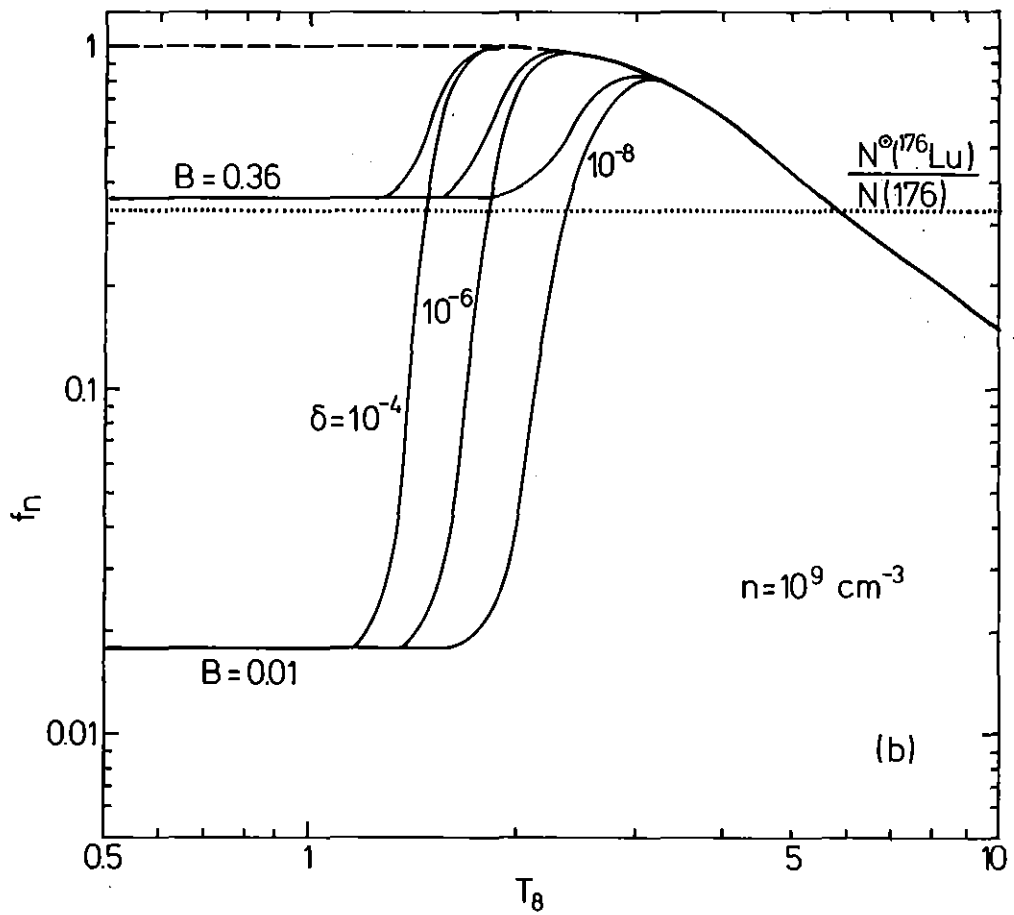
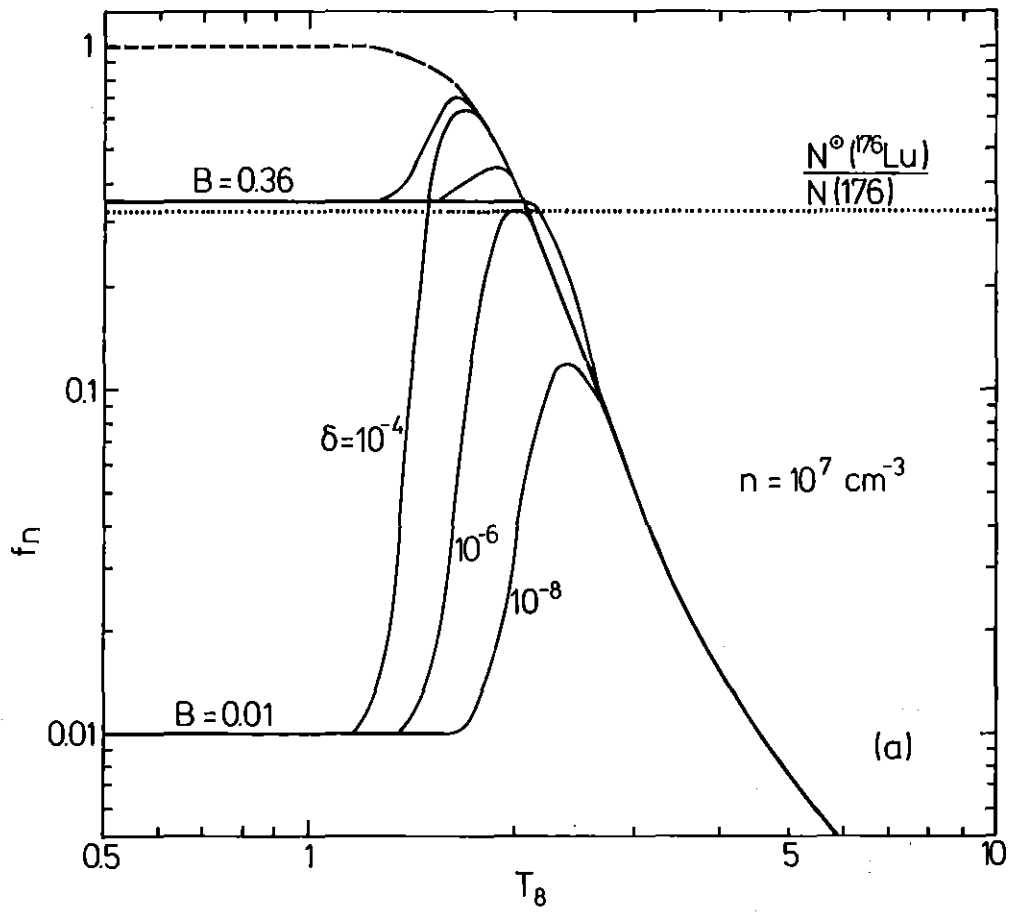


Fig. 5

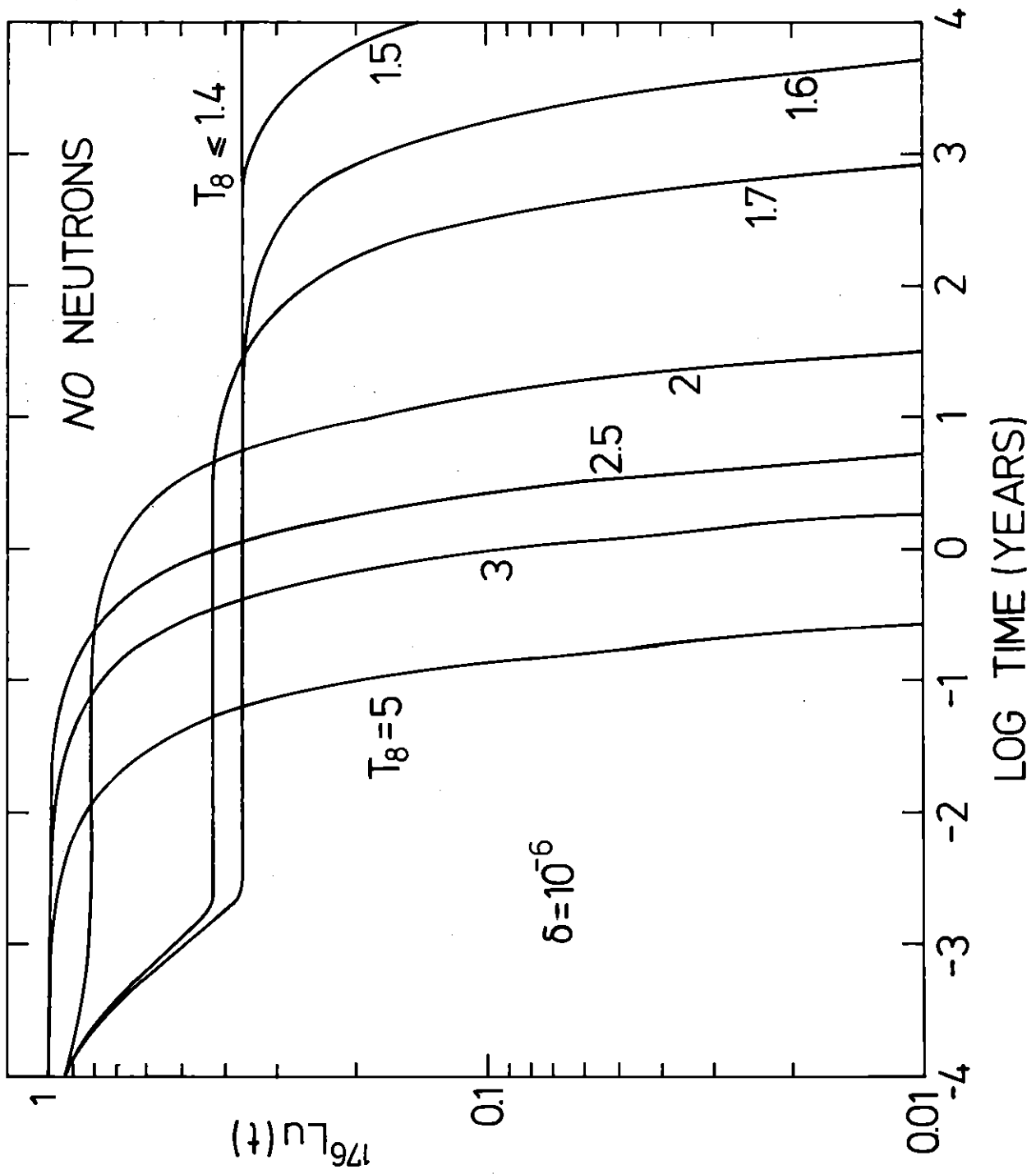


Fig. 6

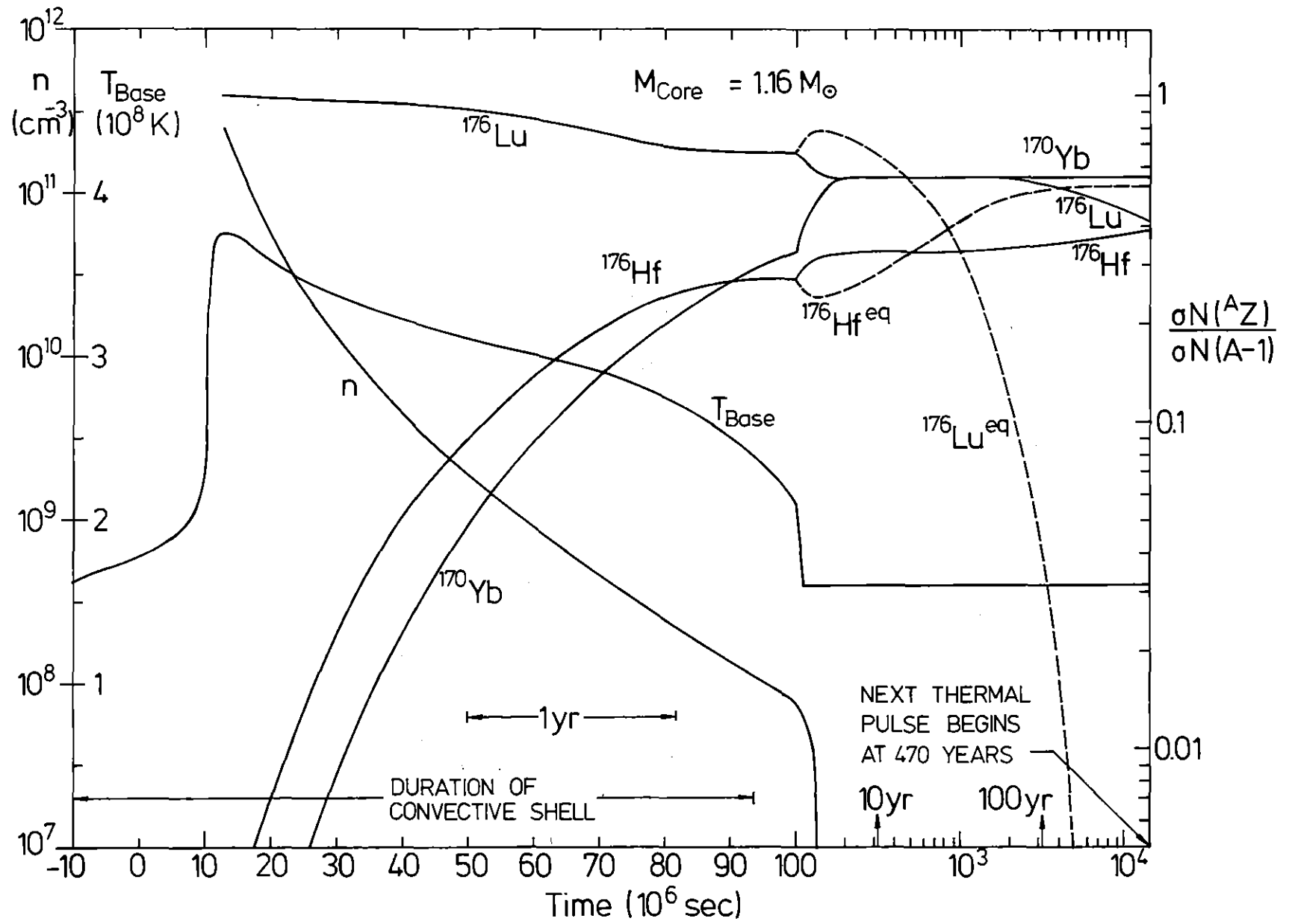


Fig. 7